OPEN BIOLOGY

royalsocietypublishing.org/journal/rsob

Research

**Cite this article:** Quiroga-Artigas G, de Jong D, Schnitzler CE. 2022 *GNL3* is an evolutionarily conserved stem cell gene influencing cell proliferation, animal growth and regeneration in the hydrozoan *Hydractinia*. *Open Biol.* **12**: 220120.
https://doi.org/10.1098/rsob.220120

Received: 27 April 2022
Accepted: 11 August 2022

**Subject Area:**
cellular biology/developmental biology

**Keywords:**
cnidarian, stem cell, *nucleostemin*, *GNL3*, *GNL3L*, CRISPR/Cas9

**Authors for correspondence:**
Gonzalo Quiroga-Artigas
e-mail: gonzalo.quiroga-artigas@crbm.cnrs.fr
Christine E. Schnitzler
e-mail: christine.schnitzler@whitney.ufl.edu

†Present address: Centre de Recherche en Biologie cellulaire de Montpellier (CRBM), Université de Montpellier, Centre National de la Recherche Scientifique, 34293 Montpellier CEDEX 05, France.

Electronic supplementary material is available online at https://doi.org/10.6084/m9.figshare.c.6167574.

THE ROYAL SOCIETY PUBLISHING

# *GNL3* is an evolutionarily conserved stem cell gene influencing cell proliferation, animal growth and regeneration in the hydrozoan *Hydractinia*

Gonzalo Quiroga-Artigas[1,†], Danielle de Jong[1] and Christine E. Schnitzler[1,2]

[1]Whitney Laboratory for Marine Bioscience, University of Florida, St Augustine, FL 32080, USA
[2]Department of Biology, University of Florida, Gainesville, FL, USA

GQ-A, 0000-0001-5954-6794; DdJ, 0000-0002-6773-723X; CES, 0000-0002-5001-6524

*Nucleostemin* (*NS*) is a vertebrate gene preferentially expressed in stem and cancer cells, which acts to regulate cell cycle progression, genome stability and ribosome biogenesis. *NS* and its paralogous gene, *GNL3-like* (*GNL3L*), arose in the vertebrate clade after a duplication event from their orthologous gene, *G protein Nucleolar 3* (*GNL3*). Research on invertebrate *GNL3*, however, has been limited. To gain a greater understanding of the evolution and functions of the *GNL3* gene, we have performed studies in the hydrozoan cnidarian *Hydractinia symbiolongicarpus*, a colonial hydroid that continuously generates pluripotent stem cells throughout its life cycle and presents impressive regenerative abilities. We show that *Hydractinia GNL3* is expressed in stem and germline cells. The knockdown of *GNL3* reduces the number of mitotic and S-phase cells in *Hydractinia* larvae of different ages. Genome editing of *Hydractinia GNL3* via CRISPR/Cas9 resulted in colonies with reduced growth rates, polyps with impaired regeneration capabilities, gonadal morphological defects, and low sperm motility. Collectively, our study shows that *GNL3* is an evolutionarily conserved stem cell and germline gene involved in cell proliferation, animal growth, regeneration and sexual reproduction in *Hydractinia*, and sheds new light into the evolution of *GNL3* and of stem cell systems.

## 1. Introduction

The study of stem cell biology has a long history and is at the forefront of research in regenerative medicine. While much of our current understanding of stem cells is based on studies performed on a small number of model organisms (e.g. model vertebrates, *C. elegans*, and *D. melanogaster*), a complete understanding of the molecular basis and evolution of stem cell systems can only be gained when looking outside the conventional experimental models [1–3].

Cnidarians have proven to be excellent experimental models to study stem cell biology and evolution, due to their morphological simplicity, cellular plasticity, outstanding regenerative capabilities, long lifespan and their key position in the phylogenetic tree as sister group to bilaterian animals [4,5]. Within the Cnidaria, hydrozoans have been widely used to gain an understanding of stem cells and regeneration processes [4–6]. Notably, hydrozoans possess a population of undifferentiated stem/progenitor cells, which are generally proliferative and migratory, named interstitial cells (i-cells) [4–8].

The hydrozoan *Hydractinia symbiolongicarpus* (hereafter *Hydractinia*) is a marine, dioecious, colonial animal that lives on the surface of hermit crab shells in the wild (figure 1*a*). Its transparency, small size, and ease of manipulation and rearing, as well as wide availability of molecular and genetic approaches, make *Hydractinia* a highly attractive research organism for experimental biology

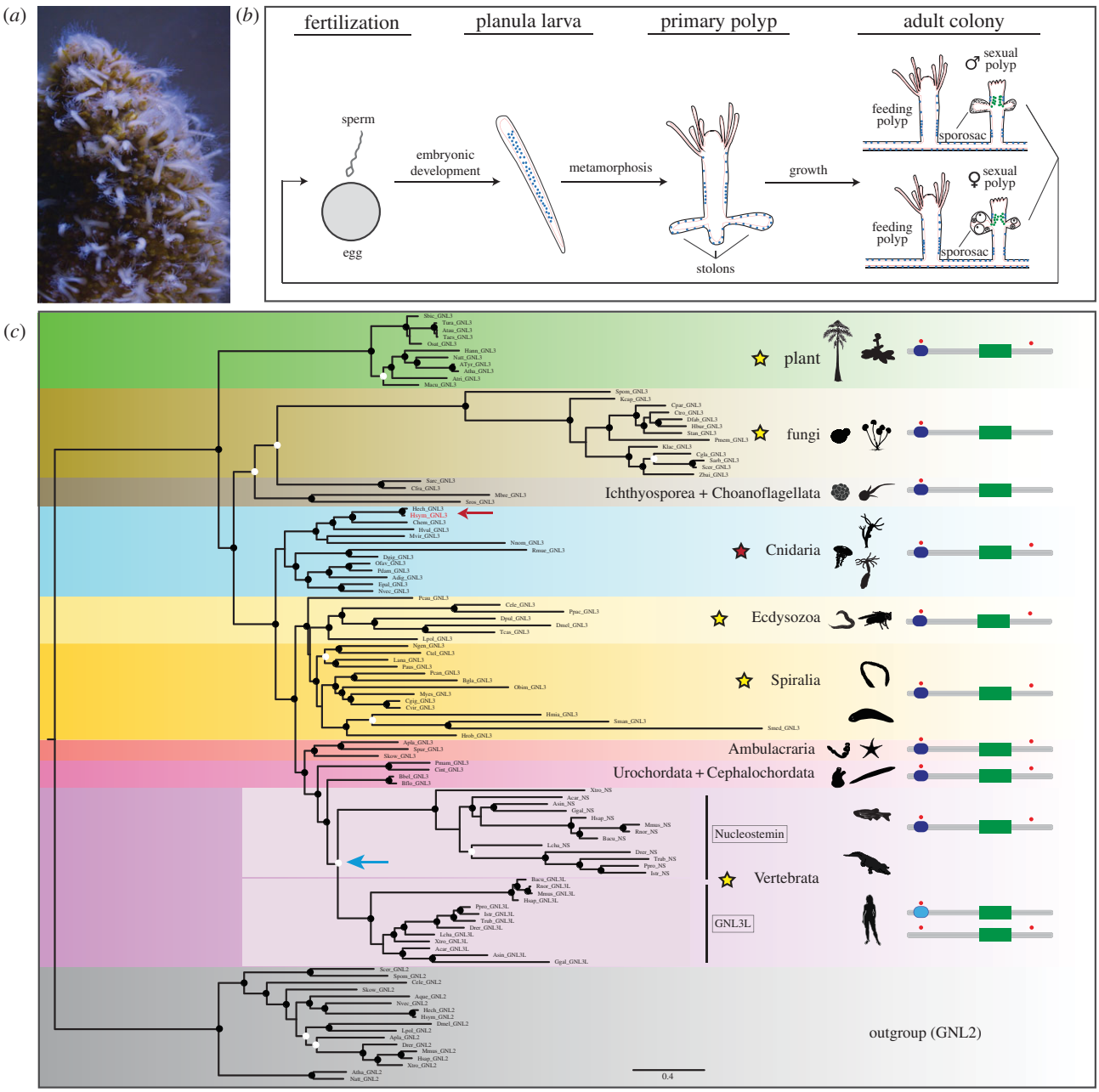


**Figure 1.** Molecular phylogeny and domain analysis of GNL3. (*a*) Photo of a *Hydractinia* colony on top of a hermit crab shell. (*b*) Schematic of *Hydractinia* life cycle. Ectodermal and endodermal epithelial layers are depicted in black and pink, respectively. I-cells are represented by blue dots and germ cells by green dots. (*c*) Maximum-likelihood (ML) phylogenetic analysis of GNL3 family of proteins (RAxML, LG + I + gamma + F; see electronic supplementary material, table S1 for full species names and accession numbers, and file S2, and S3 for input sequences and sequence alignment, respectively). Tree was rooted with GNL2 protein sequences. ML bootstrap support values (500 replicates) are shown as black circles on branch tips when support is higher than 70% and as white circles when support is higher than 50% but lower than 70%. Scale bar shows estimated number of substitutions per site. The subject of this study, *H. symbiolongicarpus* GNL3, is shown in red font and indicated by a red arrow. A putative duplication event in the vertebrate lineage, resulting in Nucleostemin and GNL3L paralogues is indicated by a blue arrow. To the right of the tree, stars indicate phyla/supergroups where at least one study has been conducted, including this study. On the far right, schematics of the domain structure of representative GNL3 proteins are shown. Grey bar indicates entire length of protein, dark blue rounded rectangle represents presence of a GN3L_Grn1 putative GTPase domain, and green rectangle represents presence of a MMR1_HSR1 50S ribosome-binding GTPase domain. Light blue rounded rectangle in the domain structure of vertebrate GNL3L indicates a derived GN3L_Grn1 putative GTPase domain, while other vertebrate GNL3L proteins lack the domain entirely. Red circles indicate the presence of at least one nuclear localization signal (NLS) in regions close to the N-terminus and C-terminus. Schematics are not to scale. Animal, plant and fungi silhouettes were taken from http://phylopic.org.

[9]. I-cells in *Hydractinia* derive from the embryonic endoderm, are found both in larval and adult stages (figure 1*b*), and are capable of giving rise to all somatic lineages as well as to germ cells [7,8,10]. It is currently unknown whether *Hydractinia* i-cells exist as a uniform population of pluripotent stem cells or as heterogeneous sub-populations of undifferentiated cells with mixed potencies. To date, in-depth functional analyses of *Hydractinia* i-cell genes are scarce [10–13], and none has been functionally characterized throughout the *Hydractinia* life cycle. Performing reverse genetics on *Hydractinia* i-cell genes and studying their function at different life cycle stages will shed light on the molecular basis and evolution of stem cell systems.

G protein Nucleolar 3 (GNL3) is a nucleolar protein that belongs to the YlqF/YawG GTPase family, which is characterized by the presence of an MMR1_HSR1 domain of five

circularly permuted GTP-binding motifs [14]. The *GNL3* gene is present as a single copy in non-vertebrate eukaryotes. A presumptive duplication event in the vertebrate clade gave rise to two paralogues, *nucleostemin* (*NS*) and *GNL3-like* (*GNL3L*) [14,15] (figure 1*c*).

The *NS* gene is highly expressed in cells capable of continuous proliferation such as different types of stem cells, including embryonic and adult neuronal stem cells, primordial germ cells, and tumour cells [14,16]. Moreover, NS contributes to biological processes such as embryogenesis, tissue regeneration and cancer development [17], making *NS* a target gene for stem cell and cancer research, as well as for regenerative and reproductive medicine. NS is capable of shuttling between the nucleolus and the nucleoplasm depending on its GTP binding state [18], and interacts directly or indirectly with a large number of proteins [14,15]. NS is involved in a variety of cellular functions such as cell cycle regulation and self-renewal [14,15,17,19], genome integrity [20,21] and ribosomal biogenesis [22–24], and can act as a reprogramming factor [19], altogether making NS a multifunctional protein essential for stem cell regulation.

The vertebrate *NS* paralogue, *GNL3L*, has been less studied overall. Unlike *NS*, *GNL3L* shows lower expression in stem cells and higher expression in differentiated tissues, although it is found upregulated in some cancers [14]. GNL3L is also able to shuttle between the nucleolus and the nucleoplasm, with a shorter nucleolar residence than NS [18]. GNL3L has been shown to regulate cell cycle transitions [25,26], negatively regulate telomere length [27], modulate the transcriptional levels of oestrogen-related receptors [28], and mediate pre-ribosomal RNA processing [24].

Invertebrate *GNL3* is a term that is used to refer to the *GNL3* gene from invertebrate animals, but also from organisms of other kingdoms like fungi and plants [17]. *GNL3* was recently identified as one of 195 genes found to have enriched expression in multipotent stem cells across several invertebrate animals, including the sponge *Spongilla lacustris*, the cnidarian *Hydra vulgaris*, the planarian *Schmidtea mediterranea*, and the schistosome *Schistosoma mansoni* [29]. Only a limited number of functional studies have been performed on invertebrate *GNL3*, however, and these have mostly been focused on typical model organisms. In *Saccharomyces cerevisiae*, GNL3 (Nug1p) is necessary for its viability and for 60S ribosomal subunit export [30], while in *Saccharomyces pombe*, GNL3 (Grn1p) is required for growth, pre-ribosomal RNA processing, and nucleolar export of pre-ribosomal complexes [31]. In *D. melanogaster*, GNL3 (NS1) is crucial for larval and pupal development, for the nucleolar release of large ribosomal subunits, and for the maintenance of larval midgut precursor cells [32]. In *C. elegans*, GNL3 (NST-1) is needed for larval growth, germline stem cell proliferation, and is involved in ribosome biogenesis [33]. In the planarian *S. mediterranea*, *GNL3* (*Nucleostemin*) is needed for complete head and tail regeneration [34]. In *Arabidopsis thaliana*, *GNL3* (*nsn1*) is highly expressed in embryos, in shoot and floral apical undifferentiated (meristematic) cells, and in developing leaves and flowers [35,36], and is required for the maintenance of inflorescence meristem identity, embryonic development, cell proliferation, plant growth, fertility and ribosome biogenesis [35–38]. Importantly, despite this evidence of *GNL3* stem cell and germ cell expression and function in these organisms, the current evolutionary paradigm that has been proposed is that vertebrate *GNL3L* is the direct descendant of invertebrate *GNL3* and that *NS* arose as a novel gene with new functions during vertebrate evolution [17,24].

Here, we identify and characterize *GNL3* in the hydrozoan cnidarian *Hydractinia* as an evolutionarily conserved stem cell gene. We show that *GNL3* is expressed in i-cells throughout the *Hydractinia* life cycle, as well as in the germline. Gene functional analyses demonstrate that *GNL3* disruption affects cell proliferation, colony growth, polyp head regeneration and sperm motility. By performing a broad cross-kingdom molecular phylogeny and domain analysis of GNL3 amino acid sequences, we show that a domain named GN3L_Grn1, located near the N-terminus is shared between invertebrate GNL3 and vertebrate NS, but is mostly absent in the NS paralogue GNL3L. We discuss how our findings contrast with the current paradigm of *GNL3* gene evolution and propose an alternative evolutionary scenario. Our study helps to highlight the importance of *GNL3* in cancer and stem cell research, as well as the significance of studying diverse animals, and of performing wide phylogenetic comparisons, to better understand gene evolution.

## 2. Results

### 2.1. GNL3 molecular phylogeny and domain analysis

Homologues belonging to the YlqF/YawG GTPase family (GNL3, GNL2, LSG1, MTG1) were identified from BLAST searches of the *Hydractinia* genome and transcriptome databases (https://research.nhgri.nih.gov/hydractinia/). We could not find a *Hydractinia* orthologue of GNL1. Protein cluster map analyses demonstrate the high sequence conservation of *Hydractinia* GNL3, GNL2, and LSG1 to other animal orthologues of the same gene subfamilies (electronic supplementary material, figure S1).

Detailed phylogenetic analyses of GNL3 amino acid sequences encompassing different kingdoms, superphyla, phyla, and subphyla were performed using maximum likelihood (figure 1*c*). The GNL2 subfamily of proteins was used as the outgroup. In preliminary analyses we included sequences from additional non-bilaterian groups (ctenophore, sponge, placozoa) but these sequences tended to have a shifting placement within the trees with low levels of support that also caused some minor rearrangements in other parts of the tree (electronic supplementary material, figure S2). Since their position in the tree was ambiguous and somewhat disruptive to tree structure, we decided to exclude them from our final phylogeny. A single copy of GNL3 is present in plants, fungi, protists and invertebrate animals. For the most part, the GNL3 tree we constructed is congruent with our current understanding of the species tree for the clades included in the analysis. This congruence is typical when there is a single copy of the gene for every species included without duplications or losses. The *Hydractinia* GNL3 sequence falls within the hydrozoan cnidarian group, as expected. Our tree supports the putative duplication event in the vertebrate clade which led to the formation of the paralogues GNL3L and NS, and all vertebrates we surveyed had both paralogues which group in their own clades (figure 1*c*).

While focusing on protein sequence comparisons, *Hydractinia* GNL3, as well as other invertebrate GNL3 sequences,

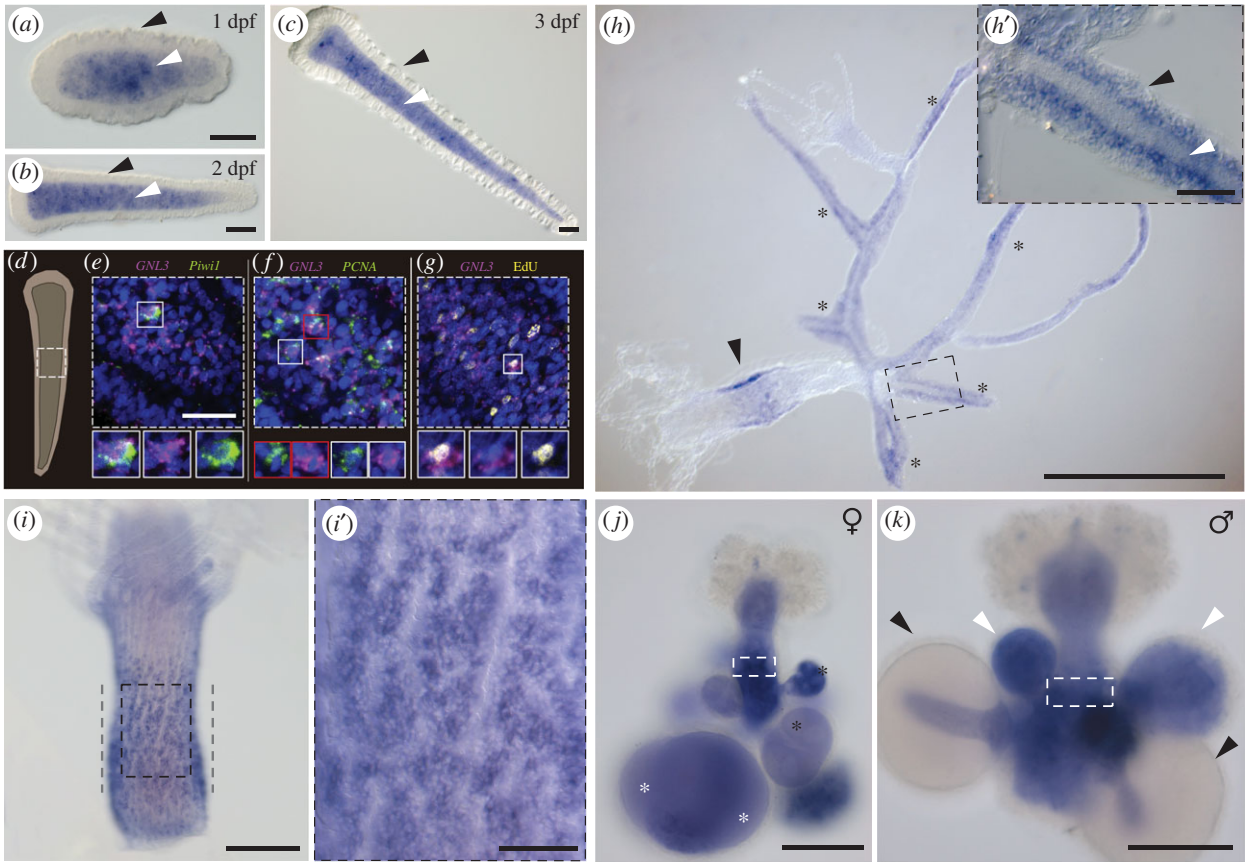


**Figure 2.** Whole mount ISH of *GNL3* in *Hydractinia*. (*a–c*) *GNL3* expression in 1 dpf, 2 dpf and 3 dpf *Hydractinia* larvae is detected in the larval endoderm (white arrowheads) but not in the larval ectoderm (black arrowheads). (*d*) Schematic of a 2 dpf larva. White square defines approximately the larval region imaged in (*e–g*). (*e,f*) Double fluorescent ISH showing co-expression of *GNL3* (magenta) and *Piwi1* or *PCNA* (green) in a subset of larval endodermal cells. (*g*) Fluorescent ISH of *GNL3* co-stained with EdU (yellow) showing some larval endodermal cells labelled with both markers. For (*e–g*), nuclei are in blue, and examples of co-expression/co-staining are indicated by white and red boxes. (*h*) *GNL3* expression in a young colony with expression in the primary polyp (arrowhead) and stolons (asterisks). (*h′*) Magnification of region outlined in (*h*) showing *GNL3* expression in the stolonal epidermis (black arrowhead) but not in the gastrodermis (white arrowhead). (*i*) *GNL3* expression in the i-cell band-like area (defined by grey dashed lines) of an adult feeding polyp. (*i′*) Magnification of region outlined in (*i*) showing *GNL3* expression in cell clusters. (*j*) *GNL3* expression in the germinal zone (white rectangle), in growing oocytes (black asterisks), and in fully grown oocytes (white asterisks) of female sexual polyps. (*k*) *GNL3* expression in the germinal zone (white rectangle), and in spermatogonia within small and medium-sized sporosacs (white arrowheads) of male sexual polyps. Note the absence of *GNL3* expression in mature sperm within large sporosacs (black arrowheads). ISH = *in situ* hybridization; dpf = days post-fertilization. Scale bars: 50 µm in (*a–c*, *h′*, *i′*); 25 µm in (*e–g*); 500 µm in (*h*); 100 µm in (*i–k*).

have a slightly higher overall pairwise similarity to vertebrate GNL3L than to vertebrate NS (electronic supplementary material, figure S1). Specifically, *Hydractinia* GNL3 has a 34.7% pairwise identity with human NS and a 38.4% pairwise identity with human GNL3L. Sequence identity levels, however, do not necessarily provide a full picture of how proteins evolve and need to be complemented by the study of the presence/absence of functional protein domains to better infer sequence evolution. To assess this, we performed PFAM and Motif Scan analyses and compared the domain structures of NS and GNL3L from several clades with *Hydractinia* GNL3 and other invertebrate GNL3 protein sequences. All amino acid sequences displayed a MMR1-HSR1 domain, expected in the YlqF/YawG GTPase family of proteins, and most of them had one to several nuclear localization signals (NLS) at the N-terminus, and sometimes also at the C-terminus, of their sequences (figure 1*c*). Importantly, all invertebrate GNL3 proteins (with the exception of ctenophore GNL3; electronic supplementary material, figure S2) share a GN3L_Grn1 domain at the N-terminus of the protein sequence with vertebrate NS, however this domain is often not present in vertebrate GNL3L, and when present, it is detected with low e-values by PFAM, indicating poor domain identity (figure 1*c*). These analyses strongly suggest that vertebrate GNL3L is more evolutionarily derived than vertebrate NS and that there may be more functional protein conservation between NS and invertebrate GNL3 than between GNL3L and invertebrate GNL3.

## 2.2. The *Hydractinia GNL3* gene is expressed in larval and adult i-cells, germ cells, oocytes, and spermatogonia

In *Hydractinia* larvae, i-cells are located in the endoderm and migrate through the mesoglea to the larval ectoderm during metamorphosis [7]. Labelling with 5-ethynyl-2′-deoxyuridine (EdU), a thymidine analogue that is incorporated into the DNA of cells during S-phase, confirmed that the majority of proliferating cells were present in the larval endoderm (electronic supplementary material, figure S3A-B). Whole mount *in situ* hybridization (ISH) of *Hydractinia* larvae at 1 dpf (days post-fertilization), 2 dpf and 3 dpf, revealed *GNL3* expression in a population of endodermal cells (figure 2*a–c*). Double fluorescent ISH on 2 dpf larvae using probes for *GNL3* and *Piwi1* (an i-cell marker), or *GNL3* and

*PCNA* (a cell proliferation marker), revealed that both these genes were co-expressed with *GNL3* in a subset of cells within the larval endoderm (figure 2*d–f*). Of $n = 103$ randomly chosen cells expressing either gene counted in six different larvae, 51.4% co-expressed *GNL3* and *Piwi1*, and of $n = 119$ randomly chosen cells expressing either gene counted in seven different larvae, 62.2% co-expressed *GNL3* and *PCNA*. Detection of *GNL3* probe in parallel with EdU also revealed co-labelling of these two markers in a subset of cells (figure 2*g*). Of $n = 103$ randomly chosen cells expressing the *GNL3* gene and/or showing EdU staining counted in five different larvae, 46.6% were co-labelled with *GNL3* probe and EdU. These findings suggest that larval i-cells are composed of a heterogeneous population of stem cells and that *GNL3* is expressed in a subset, partially overlapping with *Piwi1*. Our results also showed that *GNL3* is often expressed in cells undergoing cell proliferation within the endoderm of *Hydractinia* larvae.

We could also observe *GNL3* expression in stolons, within the interstitial region of the epidermis known to be inhabited by i-cells (figure 2*h–h'*) [39], and in the interstitial region of the epidermis in a band-like area in primary polyps (figure 2*h*) and adult feeding polyps (figure 2*i–i'*), which is also known to host i-cells and proliferating cells [11] (electronic supplementary material, figure S3C-D). Based on the spatial location and the large nuclear to cytoplasmic ratio of the *GNL3*-expressing cells, our results strongly suggest that *GNL3* is expressed in feeding polyp and stolonal i-cells of juvenile and adult *Hydractinia* colonies.

In sexual polyps, we detected *GNL3* expression in the germinal zone bearing early germ cells [10] of both female and male sexual polyps (figure 2*j–k*; electronic supplementary material, figure S4A,B). We also found *GNL3* expressed in both growing and fully grown oocytes in all sporosacs of female sexual polyps (figure 2*j*), whereas in male sexual polyps, *GNL3* probe stained spermatogonia inside small and medium-sized sporosacs, but not the mature sperm present in larger sporosacs (figure 2*k*). When combining EdU labelling with *GNL3* fluorescent ISH in male sexual polyps, we observed complete co-localization in spermatogonia within small and medium-sized sporosacs, but the complete absence of both markers in larger sporosacs (electronic supplementary material, figure S4A). These results illustrate that *GNL3* is expressed in germ cells, oocytes, and proliferating spermatogonia of female and male sexual polyps.

## 2.3. *GNL3* knockdown reduces the number of proliferating and mitotic cells in larvae

To better understand the functions of GNL3 in larvae, we knocked down the transcript of *Hydractinia GNL3* via short hairpin RNA (shRNA) electroporation of one-cell stage embryos, then studied different cellular markers in larvae of different ages following knockdown (KD). We designed and synthesized a single shRNA targeting our gene of interest, and electroporated *Hydractinia* fertilized eggs at a concentration of 1500 ng $\mu l^{-1}$ (see methods). We decided to use a concentration of 1500 ng $\mu l^{-1}$ in contrast to the 900 ng $\mu l^{-1}$ previously published [40] since we observed slightly higher knockdown levels of the *GNL3* gene when electroporating with a higher shRNA concentration. As a negative control for these experiments, we used a scrambled sequence of the shRNA used for *GNL3* knockdown, and verified that it did not target any gene in the *Hydractinia* genome using a BLAST homology search. We obtained strikingly reduced levels of *GNL3* mRNA, as shown by qPCR, in larval samples from different ages (figure 3*a*), while observing equivalent survivorship levels between control and *GNL3* KD larvae (76.9% ± 5.6% and 76.1% ± 3.3%, respectively; $n = 7$ independent experiments).

First, to assess cell proliferation and mitosis, we performed EdU labelling (an S-phase marker), and immunofluorescence analysis with a universal phosphorylated histone H3 (PH3) antibody (a mitotic marker), in *GNL3* KD larvae and scrambled controls. We observed an overall reduction in the number of both $EdU^+$ and $PH3^+$ cells in *GNL3* KD larvae at 2, 3 and 8 dpf, which was statistically significant in all cases but one (figure 3*b–e*; electronic supplementary material, figure S5). These results suggest that a putative subpopulation of larval i-cells expressing *GNL3* present lower cell proliferation and mitotic rates when *GNL3* is knocked down.

To determine whether the lower number of S-phase and mitotic cells in *GNL3* KD larvae was simply due to a reduction in the total number of larval i-cells, we used a Piwi1 antibody, previously used as an i-cell marker for *Hydractinia* [10,11]. We observed no significant difference in the number of $Piwi1^+$ cells between *GNL3* KD and scrambled control larval samples at 2 dpf and 8 dpf (figure 3*f–g*; electronic supplementary material, figure S5E-F). Altogether, our results show that knockdown of *GNL3* decreases the number of S-phase and M-phase cells without affecting the overall number of $Piwi1^+$ i-cells in *Hydractinia* larvae. This suggests that the lower numbers of proliferating cells observed upon *GNL3* knockdown might be due to an effect on the cell cycle dynamics of i-cells, rather than a reduction in the total number of i-cells. Alternately, *GNL3* knockdown may affect the subpopulation of i-cells that do not express *Piwi1*.

## 2.4. *GNL3* knockdown does not induce spontaneous DNA damage or apoptosis in larvae and does not affect larval mature ribosomal RNA species

We sought to determine whether *Hydractinia GNL3* knockdown induced spontaneous DNA damage in larval proliferating cells. For this purpose, we used a commercial antibody against gamma-H2A.X (GH2A.X), a widely used DNA damage marker labelling double-strand breaks [20,41,42]. To artificially induce DNA damage in proliferating cells, we incubated larvae in 20 mM hydroxyurea (HU) for 3 h prior to fixation. HU treatment depletes the endogenous nucleotide pool and consequently stalls the replication fork, generating DNA damage [20,43]. We observed that HU-treated larvae presented a high number of $GH2A.X^+$ cells (with a pattern reminiscent of that shown by EdU – electronic supplementary material, figure S3A-B; S6). However, performing the same experiment on *GNL3* KD larvae in the absence of HU shows that *GNL3* KD does not induce spontaneous DNA damage in *Hydractinia* larvae of different ages, as shown by the almost complete absence of $GH2A.X^+$ cells, which was equivalent to the scrambled control (electronic supplementary material, figure S6).

To study whether *GNL3* knockdown induced cell apoptosis in *Hydractinia* larvae, we used a TUNEL assay to label apoptotic cells. We observed that, whereas DNase I-treated larvae presented a vast number of $TUNEL^+$ cells, *GNL3* KD larvae of different ages displayed an almost complete absence

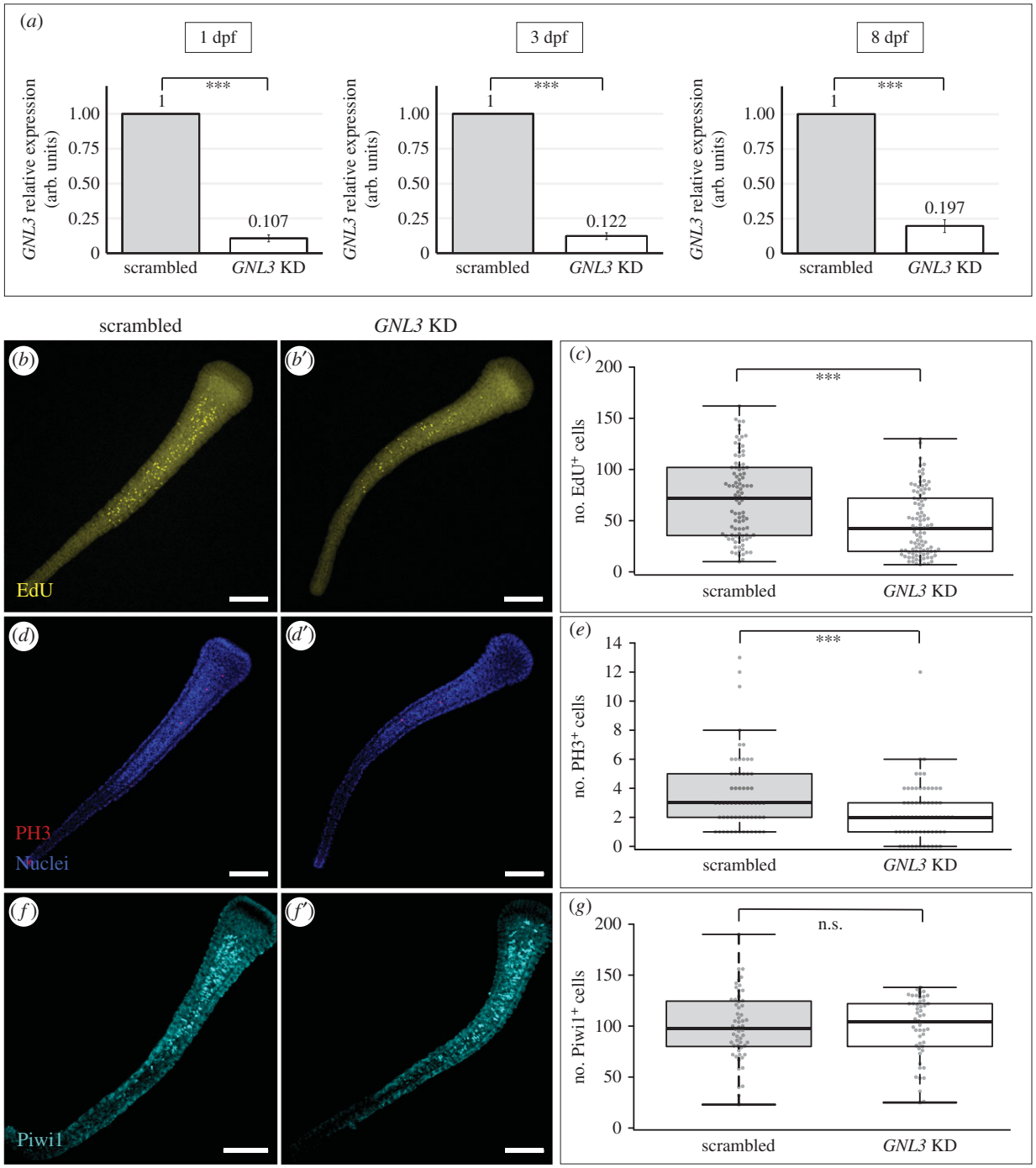


**Figure 3.** *GNL3* knockdown significantly reduces the number of EdU$^+$ and PH3$^+$ cells without affecting the number of Piwi1$^+$ cells in larvae. (*a*) RT-qPCR showing a significant decrease of *GNL3* transcript levels in *GNL3* shRNA-electroporated samples (*GNL3* KD) relative to scrambled shRNA controls at 1 dpf (left), 3 dpf (middle), and 8 dpf (right). Bar heights represent mean values of three independent experiments and error bars show standard deviations. (*b–b′*, *d–d′*, *f–f′*) Representative images of 8 dpf larvae showing EdU$^+$ cells (yellow, *b–b′*), PH3$^+$ cells (red, *d–d′*), or Piwi1$^+$ cells (cyan, *f–f′*) in scrambled and *GNL3* KD larvae. (*c,e,g*) Box plots showing the number of EdU$^+$, PH3$^+$ or Piwi1$^+$ cells for scrambled and *GNL3* KD 8 dpf larvae. Centre lines show the medians; box limits indicate the 25th and 75th percentiles (first and third quartiles); whiskers extend 1.5 times the interquartile range from the 25th and 75th percentiles; each quantified sample is represented by a grey circle. In all cases, the full depth of the larvae was imaged and images shown were projected from confocal stacks. EdU quantifications were combined from 3 independent experiments (scrambled, $n = 95$; *GNL3* KD, $n = 97$), whereas PH3 and Piwi1 quantifications were combined from 2 independent experiments (scrambled $n = 62$; *GNL3* KD, $n = 66$ for PH3; scrambled, $n = 56$; *GNL3* KD, $n = 50$ for Piwi1). n.s. = non-significant, dpf = days post-fertilization; *** = $p$-value $\leq 0.01$. All scale bars: 100 µm.

of TUNEL$^+$ cells, comparable to the scrambled control (electronic supplementary material, figure S7). This result indicates that the downregulation of *GNL3* does not induce apoptosis in *Hydractinia* larvae.

We also aimed to assess whether mature ribosomal RNA (rRNA) species (18S and 28S) were affected when *GNL3* was downregulated in *Hydractinia* larvae. We extracted total RNA from scrambled control and *GNL3* KD larvae of different ages from three independent biological replicates and used an Agilent 2100 Bioanalyzer Instrument to check the levels and ratios of mature 28S and 18S rRNA. We first observed that the levels of mature rRNA species were equivalent between conditions in all cases (electronic supplementary material, figure S8A). Next, by analysing the Bioanalyzer

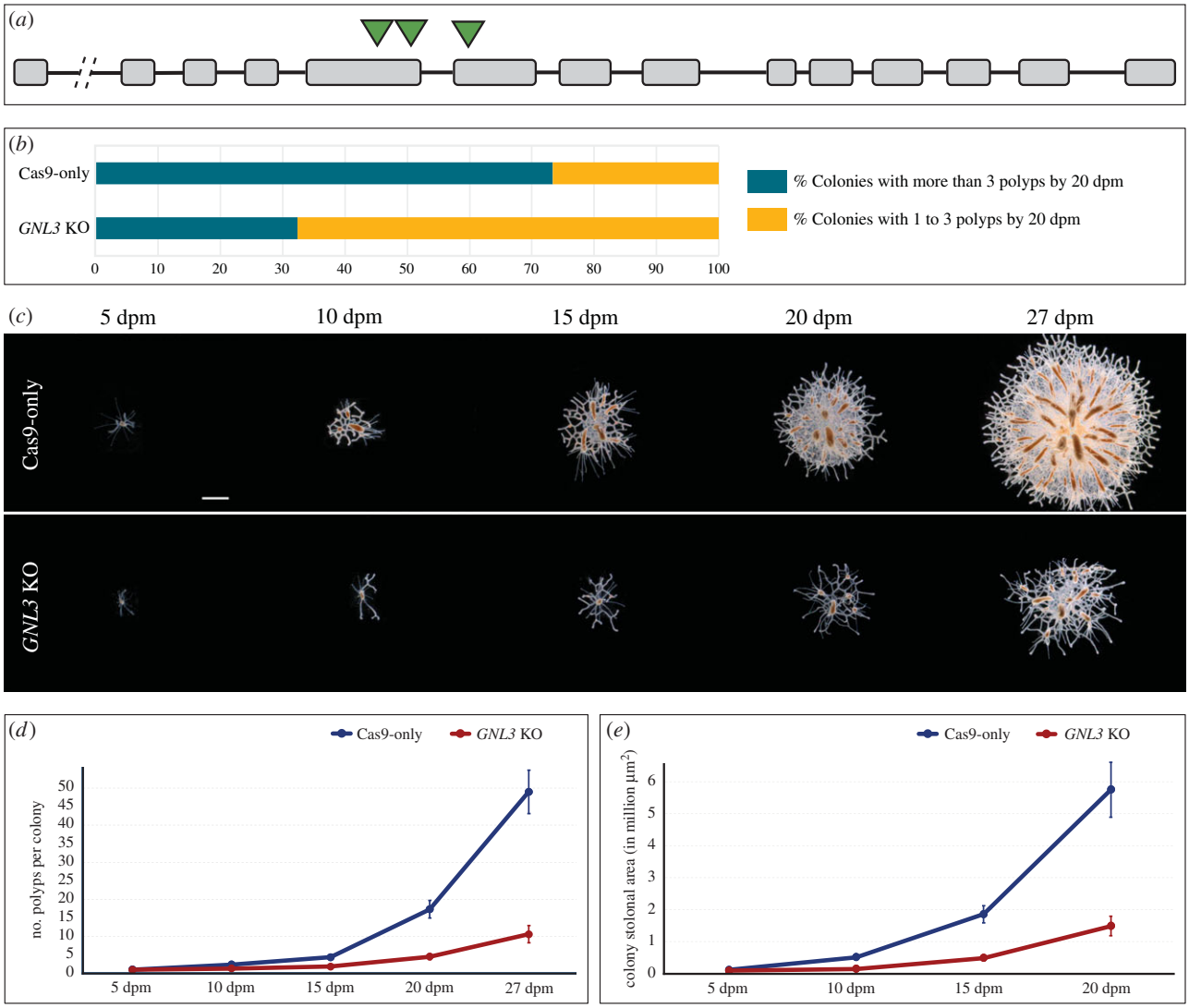


**Figure 4.** *GNL3* knockout slows colony growth. (*a*) *GNL3* gene structure depicting exons (grey boxes), introns (black lines) and target sites of sgRNAs (green triangles). Break between 1st and 2nd exon denotes several thousand base pairs of intronic region. (*b*) Graph depicting the percentage of colonies with more than 3 polyps by 20 dpm (green-blue) and the percentage of colonies with 1 to 3 polyps by 20 dpm (yellow) for Cas9-only and *GNL3* KO conditions. Fisher's exact test showed a significant difference ($p < 0.01$) between Cas9-only and *GNL3* KO samples. For Cas9-only, $n = 162$; for *GNL3* KO, $n = 178$. Data were combined from 2 independent experiments. (*c*) Representative images of Cas9-only and *GNL3* KO colonies at different timepoints post-metamorphosis. (*d*) Polyp number quantification at different timepoints in *Hydractinia* colonies for Cas9-only and *GNL3* KO conditions. (*e*) Stolonal area quantification at different timepoints in *Hydractinia* colonies for Cas9-only and *GNL3* KO conditions. In *d-e*, dots represent mean values and error bars show standard errors of the mean. Two-way ANOVA followed by *post-hoc* Bonferroni correction showed significant differences between conditions for both quantifications (electronic supplementary material, file S9). For Cas9-only, $n = 44$; for *GNL3* KO, $n = 54$. dpm = days post-metamorphosis. Scale bar = 1 mm.

electropherogram outputs, we obtained non-significant differences ($p$-values > 0.1) in the 28S/18S rRNA ratios between conditions at all timepoints (for 2 dpf samples: scrambled 28S/18S = 2.03 ± 0.06; *GNL3* KD 28S/18S = 2.13 ± 0.21; for 3 dpf samples: scrambled 28S/18S = 1.87 ± 0.06; *GNL3* KD 28S/18S = 1.97 ± 0.15; for 8 dpf samples: scrambled 28S/18S = 2.00 ± 0.17; *GNL3* KD 28S/18S = 2.07 ± 0.25; electronic supplementary material, figure S8B-D). These results strongly suggest that the biosynthesis of mature rRNAs is not altered when *GNL3* is downregulated in *Hydractinia* larvae.

## 2.5. *GNL3* knockout hinders colony growth

Since the effects of a gene knockdown are transient, generally lasting for less than two weeks in *Hydractinia* [10,40], to test the phenotypic effects of disrupting *GNL3* in *Hydractinia* colonies over a longer term, we opted to create *GNL3* knockout (KO) lines using CRISPR/Cas9 technology. Genome editing via CRISPR/Cas9 has previously been successfully deployed in *Hydractinia*, achieving knockout lines for targeted genes [10,44]. The *Hydractinia GNL3* gene consists of 14 exons and 13 introns. The overall GC content of the gene, including introns and exons, is 33.9% and that of the coding region is 40.2%. We designed three different CRISPR single guide RNAs (sgRNAs) targeting the 5th and 6th exons of the *GNL3* gene (figure 4*a*). We microinjected Cas9 protein and a mixture of the three sgRNAs into unfertilized eggs, followed by fertilization (see methods). In parallel, we injected Cas9 protein without sgRNAs as our negative control (Cas9-only). We designed primers flanking the targeted region of *GNL3* (electronic supplementary material, figure S9A) and performed PCRs using genomic DNA samples from individual larvae developed from embryos injected with sgRNA/Cas9 complexes. We observed that all larvae presented *GNL3* gene editing, albeit in all cases mosaic

(electronic supplementary material, figure S9B), indicating that our strategy was efficient in inducing mutations of our target gene. We used the inherent mosaicism of the F0 lines to our advantage since a full knockout of *GNL3* might have provoked embryonic lethality, similar to what occurs upon *NS* depletion in mice [19,45], deterring our ability to study its function.

A subset of embryos injected with sgRNA/Cas9 complexes and Cas9-only controls were reared to 21 dpf and subsequently labelled with EdU to assess changes in cell proliferation. In agreement with what we observed with younger larvae in our *GNL3* knockdown experiments (see above), we noted a significant reduction in the number of $EdU^+$ cells in our *GNL3* KO larvae compared to Cas9-only controls (electronic supplementary material, figure S10). These results showed that we could phenocopy the effects of *GNL3* KD on cell proliferation in our *GNL3* KO larvae, which encouraged us to perform phenotypic analyses on adult colonies.

To study a potential *GNL3* KO phenotype related to colony growth, we metamorphosed 3dpf larvae injected with sgRNA/Cas9 complexes or Cas9-only and obtained 92–98% metamorphosis success in both control and *GNL3* KO animals. This indicated that larval metamorphosis is not affected when the *GNL3* gene is disrupted. We then counted the percentage of colonies that presented more than 3 polyps by 20 dpm (days post-metamorphosis) and observed a much higher percentage of these colonies in the Cas9-only controls than in the *GNL3* KO animals (figure 4*b*). We performed PCR analyses using genomic DNA as template to determine the correlation between colony growth impairment and *GNL3* gene editing and noted that 74% of the slow-growing colonies (colonies with 1 to 3 polyps by 20 dpm) from *GNL3* knockouts correlated to some level of *GNL3* gene editing. Genotyping by sequencing multiple clones from three different sexually mature colonies that presented slow growth (named 1.G2, 6.F3L and 6.K2B) revealed multiple deletions in the *GNL3* gene, which produced non-sense and missense mutations when *in silico* translation on the mutant sequences was performed. In each, the wild-type (WT) *GNL3* sequence was also detected, making these colonies mosaic *GNL3* mutants (electronic supplementary material, figure S11). Lastly, we conducted a time series experiment where we took images of control and *GNL3* KO colonies at different timepoints up to 27 dpm, and quantified the number of polyps present in each colony as well as the stolonal area (figure 4*c*). *GNL3* KO colonies showed a significant reduction in both growth parameters when compared to control colonies (figure 4*d–e*). Altogether, these results demonstrate that GNL3 plays a role in normal *Hydractinia* colony growth.

## 2.6. Polyp head regeneration is impaired in *GNL3* knockout colonies

Under optimal conditions, *Hydractinia* feeding polyps are capable of fully regenerating a functional head following decapitation within approximately 72 h (figure 5*a*; [11]). To test the potential involvement of GNL3 in *Hydractinia* polyp head regeneration, we first performed ISH using a *GNL3* probe in 24 hpd (hours post-decapitation) polyps and identified cells expressing *GNL3* in the i-cell band region and in the blastema (i.e. region of high cell proliferation; figure 5*b–b′*). ISH of 48 hpd polyps revealed *GNL3* expression in the band region and in the newly formed tentacle buds (figure 5*c–c′*). The *GNL3* expression pattern in regenerating polyps suggests that *GNL3* might play an important role in polyp head regeneration.

To investigate if knockout of *GNL3* had an effect on *Hydractinia* polyp head regeneration, we dissected polyps from two *GNL3* mutant colonies (1.G2 and 6.K2B) as well as from age-matched Cas9-only control colonies, decapitated them, and assessed their ability to regenerate a head. Whereas over 50% of Cas9-only polyps had fully regenerated their heads by 72 hpd, with the remaining control polyps forming tentacle buds, the polyps from the two *GNL3* KO colonies had much lower rates of regeneration by 72 hpd (figure 5*d–e*). Strikingly, almost 100% of polyps from 6.K2B colony, the slowest-growing of all *GNL3* KO colonies we bred to sexual maturity, displayed complete regeneration failure (figure 5*e*). After 5–10 days, most 1.G2 polyps did regenerate a head, but 6.K2B polyps did not and underwent aboral regeneration [11] after 2–3 weeks with minimal or no polyp budding (electronic supplementary material, figure S12). These results indicate a requirement for GNL3 during *Hydractinia* polyp head regeneration.

## 2.7. *GNL3* knockout affects sexual polyp morphology and reduces sperm motility

To gain insight into the function of GNL3 in *Hydractinia* sexual polyps, we first examined the morphology and size of the sexual polyps in the genotyped *GNL3* KO colonies (1.G2, 6.F3L and 6.K2B), which were all males. While no obvious differences in size and morphology could be observed between 1.G2 and age-matched Cas9-only control sexual polyps, we detected defects in the sporosac structure in 6.F3L sexual polyps, such as gastrodermis fusion into the epidermis, and overall smaller size as well as underdeveloped oral regions in 6.K2B sexual polyps (electronic supplementary material, figure S11). These findings suggest that GNL3 is involved in the growth and morphogenesis of male sexual polyps in *Hydractinia*.

Since we detected *GNL3* expression in germ cells and in spermatogonia (electronic supplementary material, figure S4), we analysed the sperm of our genotyped *GNL3* KO colonies, aiming to identify potential problems. All colonies were able to spawn mature sperm upon light stimulation. However, whereas sperm from 1.G2 and 6.F3L colonies did not seem to have any obvious issues, the sperm from 6.K2B colony, the one presenting the smallest sporosacs, presented an overall much lower sperm motility when compared to the sperm of an age-matched Cas9-only control colony (electronic supplementary material, video S1). This result suggests an association of GNL3 with the proper development of male gametes, the absence of which negatively affects their final motility. Alternatively, the lack of GNL3 protein in the mature sperm cells might directly affect their motility.

# 3. Discussion

To date, most GNL3 studies have been focused on vertebrate NS. By contrast, studies characterizing invertebrate GNL3 have been scarce and sporadic across organisms, and generally not completely accounted for when inferring evolutionary hypotheses regarding how invertebrate GNL3 relates to NS and GNL3L in vertebrates.

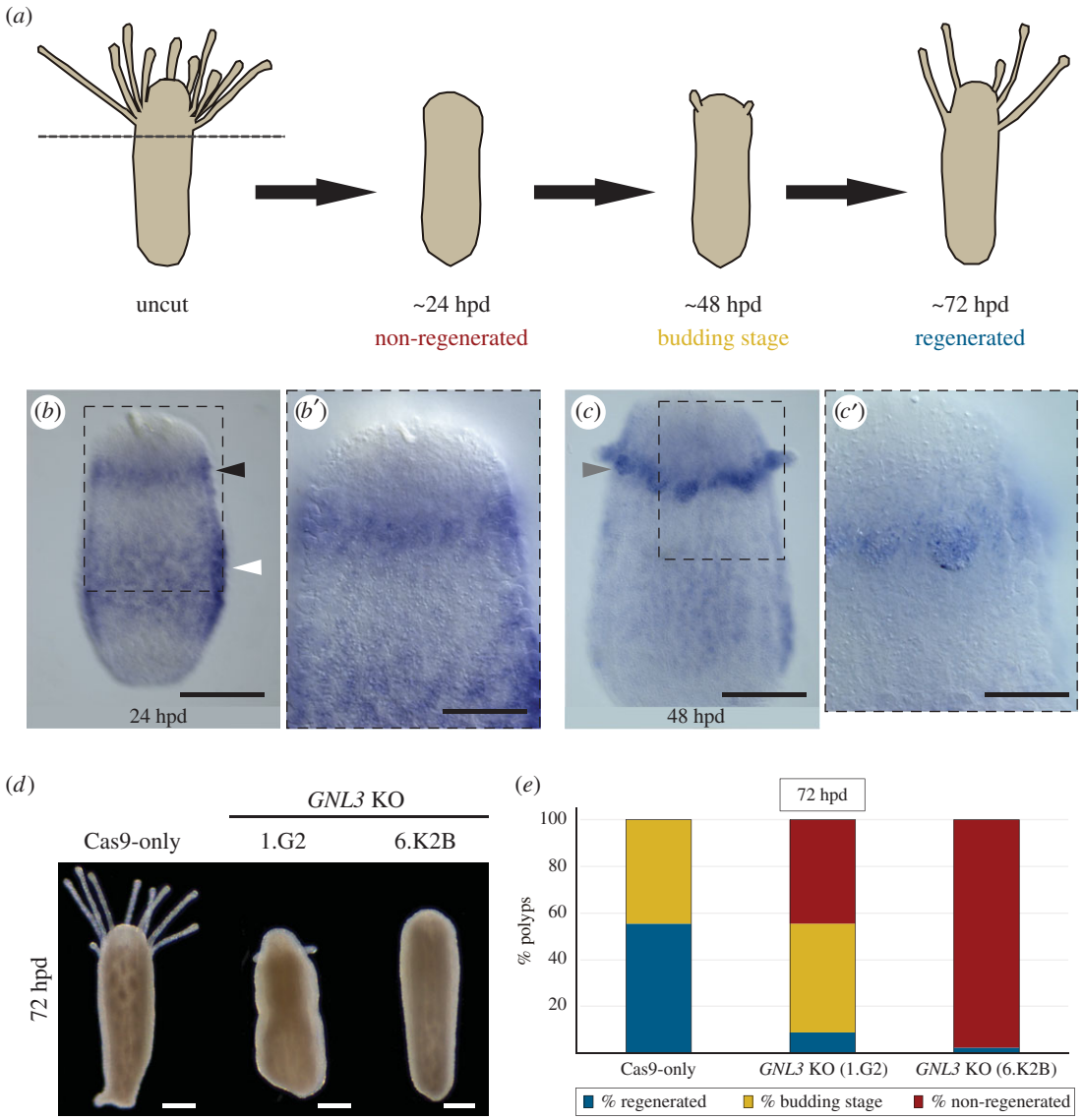


**Figure 5.** *GNL3* knockout impacts polyp head regeneration. (*a*) Schematics depicting *Hydractinia* feeding polyp head regeneration dynamics. Dotted grey line indicates position of decapitation. By 24 hpd polyps have not yet regenerated a head. By 48 hpd, new tentacle buds have formed. In about 72 hpd, polyps have regenerated a functional head with mouth and tentacles. (*b*) ISH detection of *GNL3* mRNA in the band area (white arrowhead) of a 24 hpd feeding polyp, as well as in the blastema region (black arrowhead). (*b*′) Magnification of region outlined in (*b*). (*c*) ISH showing *GNL3* expression concentrated in the regenerating tentacle buds (grey arrowhead) of a 48 hpd feeding polyp. (*c*′) Magnification of region outlined in (*c*). (*d*) Representative images of 72 hpd polyps from a Cas9-only control colony and from two *GNL3* KO colonies (1.G2 and 6.K2B). Note the slower or absent head regeneration in the *GNL3* KO colonies when compared to the control. (*e*) Stacked bar graph depicting the percentage of decapitated polyps that have regenerated (blue), are in a budding stage (yellow), or have not regenerated (red) by 72 hpd. In all cases, $n = 45$ decapitated polyps. Data were pooled from three independent experiments. hpd = hours post-decapitation. Scale bars: 100 µm in (*b*,*c*); 50 µm in (*b*′,*c*′); 200 µm in (*d*).

We show that *GNL3* is expressed in *Hydractinia* stem cell and germline populations, and demonstrate its involvement in cell proliferation, animal growth, regeneration and sperm motility. Our study opens new paths for a better understanding of the role of *GNL3* in *Hydractinia* i-cells, and more broadly, of stem cells and their evolution.

## 3.1. Invertebrate GNL3 paradigm shift

Based on the fact that human and mouse NS could not rescue the *GNL3* mutant phenotype in *S. pombe* and *C. elegans*, respectively [31,33], but human GNL3L could rescue it in S. *pombe* [31], and on the involvement of invertebrate GNL3 in ribosome biogenesis [31–33], it has been proposed that vertebrate *GNL3L* is the homolog of invertebrate *GNL3* [17,24]. We argue that this evidence is not enough to claim that invertebrate *GNL3* is more functionally related to *GNL3L* than it is to *NS*:

(1) Rescue experiments with gene/protein expression from other organisms of distant phylogenetic position (i.e. xenorescues) do not always work, likely due to functional divergence or modification of binding sites occurring during sequence evolution.
(2) In the *S. pombe* study [31], the expression of the closely related *S. cerevisiae GNL3* (*nug1*) could not rescue the growth defect phenotype of *GNL3* (*Grn1*) mutants, while the distantly related human *GNL3L* could partially restore it. This paradoxical result suggests a divergent evolution of the gene *GNL3* in this yeast species (supported by our phylogeny; figure 1*c*), making it appear

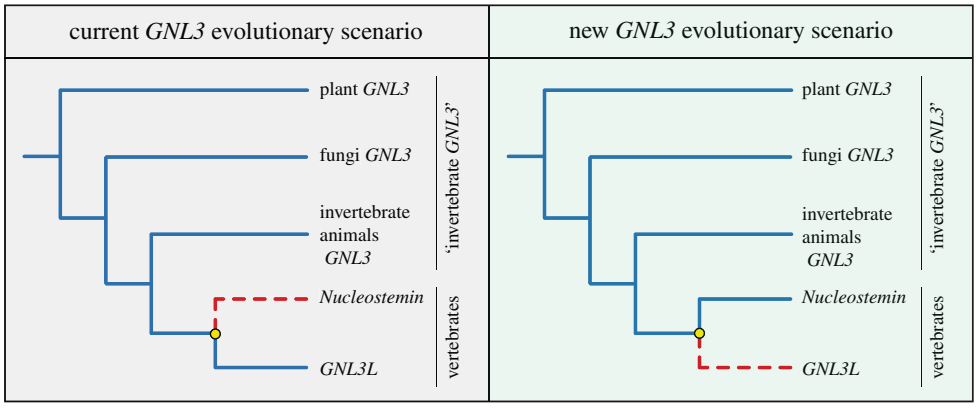


**Figure 6.** *GNL3* gene evolutionary scenarios. Left, current *GNL3* evolutionary scenario based on [17,24]: Vertebrate *GNL3L* is hypothesized to be the direct descendant of invertebrate *GNL3*, and *Nucleostemin* arose as a novel gene with new functions following a duplication event during vertebrate evolution (yellow circle). Right, proposed new *GNL3* evolutionary scenario: Vertebrate *Nucleostemin* is the direct descendant of invertebrate *GNL3*, and *GNL3L* arose as a novel gene with new functions following a duplication event in the vertebrate clade (yellow circle).

to be more functionally similar to human *GNL3L* than to the closely related *S. cerevisiae GNL3* and to human *NS*.

(3) Interestingly, *D. melanogaster* and *C. elegans* GNL3 sequences do not cluster with GNL3L nor with NS protein families (electronic supplementary material, figure S1). This implies that *D. melanogaster* and *C. elegans GNL3* genes, while studied more in-depth [32,33], have also diverged the most, potentially allowing for new functions to arise and others to disappear. Moreover, plant *GNL3* studies have not been considered when inferring the current evolutionary scenario. All this highlights the necessity of studying a variety of organisms from different phyla, since the focus on model organisms could potentially obscure the complete picture of the evolution and functions of a gene.

Our broad sampling for our phylogenetic domain analysis illustrates the presence of a GN3L_Grn1 domain at the N-terminus of all invertebrate GNL3 (with the exception of ctenophores) and all vertebrate NS amino acid sequences, but the complete absence or a much lower GN3L_Grn1 domain sequence identity in vertebrate GNL3L sequences. Moreover, invertebrate GNL3 and NS sequences show a higher similarity in the presence and distribution of NLS sequences than they do to GNL3L. Overall, the most parsimonious evolutionary explanation is that invertebrate GNL3 and vertebrate NS share common ancestry and that GNL3L arose secondarily as a novel gene during the vertebrate duplication event, becoming more evolutionary derived, contrary to what has been previously suggested [17,24]. We thus propose a new paradigm for GNL3 evolution, where vertebrate GNL3L functionally diverged from its paralogue, NS, as well as from its invertebrate orthologue, GNL3, while NS and invertebrate GNL3 share common ancestry and thus have retained more protein domain and functional identity (figure 6).

This paradigm shift has important consequences on the interpretation of GNL3 functional evolution. Based on the new paradigm we propose, GNL3L could have evolved novel functions acquired after the presumptive duplication event in the vertebrate clade, but also retained some ancestral functions that rely on the highly conserved MMR1_HSR1 domain, some of which might be redundant with its paralogue, NS. By contrast, NS and invertebrate GNL3 are more likely to share more ancestral functions, since both the GN3L_Grn1 and the MMR1_HSR1 domains have been conserved throughout evolution. In this manner, some GNL3L functions like the modulation of the transcriptional levels of oestrogen-related receptors [28], or the negative regulation of telomere length [27], are likely vertebrate GNL3L novelties, while vertebrate NS and invertebrate GNL3 involvement in other aspects such as regeneration, stemness, or genome stability might have been retained from the ancestral functions of GNL3. Further studies of invertebrate *GNL3* genes in different organisms will shed light on the evolution of GNL3, and on the paradigm shift in evolutionary scenarios we propose.

## 3.2. GNL3, growth and regeneration

Experiments with *GNL3* mutants at the organismal level have demonstrated the indispensability of GNL3 for organism growth. For example, *C. elegans GNL3* knockouts display larval growth arrest [33], and *A. thaliana GNL3* mutants exhibit growth defects in both aerial and underground organs, leading to dwarf plants [36,37]. Our results suggest that the slower growth rate observed in *Hydractinia GNL3* knockout colonies is due to reduced cell proliferation, similarly to what occurs in plants [37]. *Hydractinia GNL3* KO growth could be affected by a combination of other reasons in addition to reduced cell proliferation, however, such as impaired ribosomal subunit export leading to lower translation levels, or excessive cell differentiation; phenotypes observed in plant *GNL3* mutants [38] and in *NS* knockdowns of embryonic stem cells [19], respectively. Thus, further experimentation would be needed to specify the reason(s) for the slow growth phenotype observed in *Hydractinia GNL3* knockout colonies. A link could be made between *GNL3/NS* involvement in organismal growth ([33,36,37]; this study) and tumour growth [46,47], highlighting the potential that *GNL3/NS* downregulation could have in developing cancer therapies to reduce tumour growth. Nanoparticle drug delivery systems targeting *NS* have already been tested with successful results, obtaining smaller-sized prostate cancer tumours [47].

The biological process of regeneration has long attracted researchers, and efforts have been made to broaden the therapeutic strategies in regenerative medicine. Studies *in vivo* on emerging model organisms with high regenerative capabilities, such as cnidarians and planarians, will help decipher

the shared aspects of regeneration in multicellular organisms of different phylogenetic positions, highlighting features that are essential for regeneration [48,49]. In *Hydractinia* and planarians, head regeneration depends on cell proliferation, and the primary cellular source for blastema establishment is the migration of pluripotent stem cells (i-cells in *Hydractinia*, cNeoblasts in planarians) from the body to the prospective head [11,50,51]. Other strategies such as transdifferentiation, which occurs *in vitro* in the hydrozoan jellyfish *Podocoryne carnea* [52], or dedifferentiation, which takes place during newt lens regeneration [53] and during zebrafish heart and fin regeneration [54], have not yet been assessed during *Hydractinia* head regeneration, and thus their contribution cannot be discarded. The importance of GNL3 in regeneration processes has been illustrated by NS accumulation in dedifferentiating retinal pigmented epithelial cells during newt lens regeneration and in degenerating muscle fibres during newt limb regeneration [53], and by GNL3 requirement for complete head and tail regeneration in planarians [34]. Our results demonstrate the necessity of GNL3 for regeneration in *Hydractinia*, although the mechanism through which GNL3 functions during regeneration remains unknown. The hindered regeneration abilities of *GNL3* KO polyps could be due to impaired cell proliferation, but other aspects such as blastema formation via migration of i-cells to the wound region [11] could also be affected. Interestingly, cell migration was shown to be inhibited in several cell lines when *GNL3*/*NS* was silenced [46,55]. In combination with previous findings, our data suggest an ancient and evolutionarily conserved role of GNL3 in regeneration and infers that GNL3 might be essential for all regeneration processes, independently of the phylogenetic position of the regenerating organism, and of the cellular and molecular strategies used for regeneration. This emphasizes the relevance of GNL3 research for regenerative medicine progress.

### 3.3. GNL3 in sexual reproduction

Previous reports have illustrated the importance of GNL3 for sexual reproduction: NS was found present at high levels in mouse male germ cells, and its knockdown reduced germ stem cell proliferation potential *in vitro* [56]. Germline-specific *C. elegans GNL3* mutants were sterile, presenting defects in germline stem cell proliferation [33]. *NS* was differentially expressed in sterile *Xenopus* hybrid testes when compared to fertile non-hybrids [57]. In *A. thaliana*, *GNL3* mutants presented defects in reproductive fertility seen by the development of defective flowers, and the presence of unfertilized ovules [35,36]. We showed *GNL3* expression in *Hydractinia* germ cells, oocytes, and proliferating spermatogonia. Moreover, one outcome of *Hydractinia GNL3* gene knockout we observed was the presence of defects in sexual polyps and the spawning of impaired sperm. Therefore, our results add to the body of evidence that *GNL3* disruption has negative effects on the germline and, more generally, on sexual reproduction, thus affecting the fitness of a species.

### 3.4. GNL3 cellular functions in different phylogenetic contexts

It has been shown that vertebrate NS perturbation reduces cell proliferation and can induce cell cycle arrest [45,58–61], and that plant *GNL3* mutants present inefficient cell proliferation and impaired cell cycle progression in their meristems [37], therefore affecting cell cycle dynamics. Our results show that *GNL3* disruption reduces the number of S-phase and M-phase cells without affecting the overall number of Piwi1$^+$ cells in *Hydractinia* larvae, strongly suggesting that the cell cycle dynamics of i-cells are affected. Interestingly, Qu and Bishop, 2012 [19] demonstrated that *NS* depletion in mouse embryonic stem cells reduced the number of S-phase cells due to a lengthened G1 phase of the cell cycle, which in turn led to increased differentiation. Based on our current data, we cannot pinpoint whether a similar mechanism governs the cell proliferation phenotype we obtained. Since we detect *GNL3* in i-cells that do not appear to express *Piwi1*, it is also possible that only this subset is affected upon knockdown of *GNL3*. Further experimentation would help determine the specific cells and specific mechanisms involved.

Vertebrate *NS* depletion can induce apoptosis (i.e. programmed cell death) of different cancer and stem cell types [55,62–65] due to reduced cell viability. In *Hydractinia*, apoptosis occurs naturally as part of the metamorphosis process from larva to polyp but only takes place sporadically in a few cells during larval growth and homeostasis [66]. Our results show that apoptosis does not take place when *GNL3* gene is knocked down in *Hydractinia* larvae, even while cell proliferation is affected. This suggests that *GNL3* is not crucial for *Hydractinia* i-cell viability, possibly thanks to the plasticity of cnidarian cells [5], which might allow them to overcome the insult and avoid apoptosis.

Downregulation of vertebrate *NS* induces DNA damage since it hampers the homology-directed repair of DNA damage foci that spontaneously occur during DNA replication of stem and progenitor cells [20]. NS also plays an important role in preventing telomere damage [21]. Hence, NS carries out essential functions in genome protection of actively dividing cells. Our results show that *GNL3* knockdown does not induce spontaneous DNA damage in larval cells, but our approach does not discount the possibility that GNL3 might still be involved in DNA damage repair upon genotoxic stress. It has been proposed that the DNA damage repair function of GNL3 is a vertebrate NS innovation [17,24]. This hypothesis contrasts with the results obtained in *A. thaliana*, however, where *GNL3* mutants presented higher sensitivity to treatments with genotoxic agents [37], suggesting plant GNL3 involvement in DNA damage repair processes. Similar experiments to those performed in plants and in *Hydractinia* could be performed in a wide range of organisms to shed light on the open question of whether the DNA damage repair ability of GNL3 is ancestral, and has been conserved throughout evolution, or whether it is a vertebrate novelty.

Several lines of work have demonstrated the involvement of NS [22–24], GNL3L [24], and invertebrate GNL3 [30–33,38] in different aspects of ribosome biogenesis, such as the biosynthesis of mature rRNAs or the cytoplasmic export and assembly of 60S ribosomal subunits. Our results strongly suggest that the knockdown of *GNL3* does not affect mature rRNA biosynthesis in *Hydractinia* (contrary to what was shown for GNL3L [24]), but do not exclude the possibility that other aspects of ribosome biogenesis, such as large subunit export and assembly, could be affected. Based on the fact that NS, GNL3L, and invertebrate GNL3 have been shown to be involved in one facet or another of ribosome biogenesis, it is likely that *Hydractinia* GNL3 also has

some involvement in these processes. Further experimentation is needed to confirm this hypothesis.

Overall, invertebrate GNL3 and NS are seemingly involved in a myriad of cellular functions. These functions might vary depending on the organism, on the stem or tumour cell type, on the microenvironment surrounding *GNL3*/*NS*-expressing cells, and on particular cellular burdens such as genotoxic exposure or nucleolar stress. The fact that some interacting partners of NS, like p53 or mouse double minute 2 (MDM2) [14,15], are missing in some organisms where GNL3 is present, increases even more the complexity of the functional evolution of this puzzling stem cell gene. Nonetheless, our results, in addition to our broad phylogenetic survey of GNL3/NS functions, suggest that GNL3 has an ancient evolutionarily conserved function in stem cell regulation via the control of cell proliferation.

# 4. Opening up

It has been proposed that stem cells are not a homologous entity shared among animals of different phylogenetic clades, and that stem cell-specific regulatory networks might have evolved independently in vertebrates and cnidarians [5]. The potential homology of stem cell types between different animal clades would be supported if more evidence of evolutionarily conserved stem cell genes could be found regarding their presence and function. Thus, the identification of *GNL3* as a gene expressed in *Hydractinia* i-cells, and its presence in stem cells from both animals and plants, contrasts with the idea of stem cells evolving independently. Given the wide phylogenetic conservation of GNL3 proteins and their involvement in stem and germ cell regulation in plants and animals, we hypothesize that the ancestral *GNL3* gene might have been part of the original gene toolkit of the common ancestor of all eukaryotes. Our results, together with previous findings on *GNL3* in other organisms, suggest that the genetic control of stem cell regulation might present deep ancestry, and support a common evolutionary origin of stem cell types. More in-depth functional and mechanistic studies of the *GNL3* gene in a wide range of organisms would be invaluable to better understand its functions and the extent to which they have been conserved, shedding light into the biology and molecular basis of stem cell systems and how they have evolved.

# 5. Material and methods

## 5.1. Animal husbandry and drug treatment

*Hydractinia* spawning, embryo and larvae culturing, larval metamorphosis induction, and adult colony breeding were performed as previously described [40]. A newly optimized Monday–Friday feeding regime was established, consisting exclusively of SEP-Art Artemia nauplii (INVE Aquaculture), which were consistently enriched two times with S.presso (SELCO) the day before colony feeding.

To induce DNA damage, larvae were incubated in the ribonucleotide reductase inhibitor hydroxyurea (HU; Sigma-Aldrich, St Louis, MO. USA) at a concentration of 20 mM in Millipore-Filtered Seawater (MFSW) for 3 h.

## 5.2. Ylqf/YawG GTPase family cluster map, GNL3 molecular phylogeny and GNL3 domain analysis

To identify YlqF/YawG GTPase family genes in *Hydractinia*, tBLASTn searches were performed on *Hydractinia* genome and assembled transcriptomes, using human YlqF/YawG GTPase family protein sequences as bait. Protein sequence clustering was performed using CLANS2 [67], with a BLOSUM62 matrix and a *p*-value cutoff of $1 \times 10^{-1000}$. Sequences were retrieved from UniProtKB and by recovering the top 100 hits of BLAST searches while using each of *Hydractinia* YlqF/YawG GTPase family representatives as query. CD-HIT [68] was run with 99% identity to exclude sequence duplicates. The FASTA file containing the 1067 sequences used to obtain the cluster map (electronic supplementary material, figure S1) can be found in electronic supplementary material, file S1.

To perform GNL3 molecular phylogenetic analyses, a subset of GNL3 sequences found in electronic supplementary material, file S1 were handpicked to create a comprehensive list that encompasses plants, fungi, protists and most major animal clades (a number of GNL3 sequences not present in file S1 were retrieved from available online genomic and transcriptomic sources and added to the phylogenetic analyses; GNL2 sequences were also added to be used as outgroup; electronic supplementary material, file S2). To generate the tree shown as figure 1*c*, a total of 112 full-length protein-coding sequences were aligned automatically using MAFFT v. 6.861b with the linsi options [69]. The final alignment file is provided in electronic supplementary material, file S3. ProtTest 3 [70] which calls PhyML for estimating model parameters [71] was used to select the best-fit model of protein evolution for the alignment, which was LG + I + gamma + F ('LG' indicates the substitution matrix, 'I' specifies a proportion of invariant sites, 'gamma' specifies gamma-distributed rates across sites, and 'F' specifies the use of empirical amino acid frequencies in the dataset). Maximum-likelihood (ML) analyses were performed using RaxML v. 8.2.9 [72]. ML branch support was estimated using non-parametric bootstrapping (500 replicates). The resulting tree was rooted with the GNL2 clade in FigTree v. 1.4.4 (http://tree.bio.ed.ac.uk/software/figtree/) and compiled in Adobe Illustrator. The same pipeline was followed to generate the tree shown as electronic supplementary material, figure S2, where a total of 115 full-length protein-coding sequences were selected and aligned as described above (electronic supplementary material, file S4 and S5). In that case, the best-fit model was JTT + gamma.

To analyse the different GNL3, GNL3L and NS protein domains, we used the respective amino acid sequences from a broad subset of organisms belonging to each clade of the phylogenetic analyses shown in figure 1*c* as query. Additionally, amino acid sequences of *A. queenslandica*, *T. adhaerens* and *M. leidyi* were also analysed (electronic supplementary material, figure S2; electronic supplementary material table S1). Domain analyses were performed using PFAM (https://pfam.xfam.org/) and Motif Scan (https://myhits.sib.swiss/cgi-bin/motif_scan).

## 5.3. *In situ* hybridization

For colorimetric *in situ* hybridization, all samples were first relaxed in 4% $MgCl_2$ 1 : 1 MFSW-mq$H_2O$ for 20 min, and

then fixed in Fix 1 (4% PFA + 0.2% glutaraldehyde + 0.1% Tween-20 in MFSW) for 90 s at room temperature. This was followed by removal of Fix 1 and incubation in ice-cold Fix 2 (4% PFA + 0.1% Tween-20 in MFSW) for 90 min at 4°C. After fixation, three washes of 15 min in ice-cold PBS containing 0.1% Tween-20 (PTw) were performed. For permeabilization and storage, samples were dehydrated in increasing concentrations of methanol in PTw (25%, 50%, 75%, 100%), and stored at −20°C for at least 24 h. Samples were rehydrated by decreasing concentrations of methanol in PTw (75%, 50%, 25%) and washed three times in PTw. Samples were then placed in a heat block at 85°C for 20 min to inactivate endogenous alkaline phosphatases. This step was followed by 10-minute washes with 1% Triethanolamine in PTw, then with 6 µl $ml^{-1}$ and 12 µl $ml^{-1}$ acetic anhydride diluted in 1% Triethanolamine-PTw. After several washes in PTw, samples were transferred into a 24-well plate and pre-hybridized in hybridization buffer (4M urea, 5× SSC pH 7.0, 1% SDS, 0.1% Tween-20, 100 ug $ml^{-1}$ tRNA and 50 ug $ml^{-1}$ heparin in DEPC-treated mq$H_2O$) without probes for 2–5 h at 55°C. After pre-hybridization, Digoxigenin-labelled antisense RNA probe for *GNL3* was preheated at 90°C for 10 min and added to fresh hybridization buffer immediately before incubation with the samples at 55°C for 36–60 h. Following hybridization, samples were washed with decreasing concentrations of hybridization buffer in 2× SSC (at 55°C), followed by decreasing concentrations of 0.2× SSC in PTw (at room temperature). After post-hybridization washes, two 10-minute washes in maleic acid buffer (-MAB- 100 mM Maleic acid, 150 mM NaCl, pH 7.5) containing 0.1% Triton X-100 (MABT) followed. Samples were then blocked in blocking solution (1/10 Roche Blocking Buffer, ref. 11096176001, in MAB) for at least one hour at room temperature, followed by antibody incubation (Anti-Digoxigenin-AP, Fab fragments; Sigma-Aldrich) at 1 : 5000 dilution in blocking solution, overnight at 4°C. The following day, samples were washed six times in MABT and then incubated in alkaline phosphatase (AP) buffer (100 mM NaCl, 50 mM $MgCl_2$, 100 mM Tris -pH 9.5 and 0.5% Tween-20 in mq$H_2O$) containing 0.33 mg $ml^{-1}$ NBT and 0.165 mg $ml^{-1}$ BCIP. This solution was refreshed every 1–2 h during the first day of development and twice a day the following days. When desired, the reaction was stopped by washing samples several times in PTw. Samples were mounted in TDE (97% 2,2′-Thiodiethanol and 3% 1× PBS) before microscopy.

For larvae double fluorescent *in situ* hybridization, samples were fixed, stored and treated as for colorimetric ISH unless noted otherwise. Hybridization was performed using a Digoxigenin-labelled probe for *GNL3* and a Fluorescein-labelled probe for *Piwi1* or *PCNA*. Following post-hybridization washes, endogenous peroxidase activity was quenched by incubating samples twice for 30 min in 3% $H_2O_2$ at room temperature. Samples were first incubated overnight at 4°C with an antibody Anti-Digoxigenin-POD, Fab fragments (Sigma-Aldrich) at 1 : 1500 dilution in blocking solution. Samples were washed six times in MABT, then washed in PTw for 45 min, and incubated in tyramide development solution (2% dextran sulfate, 0.0015% $H_2O_2$, 0.2 mg $ml^{-1}$ iodophenol and 1× Alexa Fluor 594 Tyramide reagent -B40957- in PTw) for 10 min at room temperature. After five 15-minute washes in PTw, fluorescence was quenched with 100 mM glycine solution (pH 2.0) for 10 min at room temperature and washed again four times in PTw. Overnight incubation at 4°C with an antibody Anti-Fluorescein-POD, Fab fragments (Sigma-Aldrich) at 1 : 1500 dilution in blocking solution was followed by washes in MABT, PTw and tyramide development solution as before (containing 1× Alexa Fluor 488 Tyramide reagent (B40953) in place of Alexa Fluor 594). Nuclei were stained using Hoechst 33342 and samples were mounted in Fluoromount (Sigma-Aldrich) before confocal imaging analysis. Primers used for probe synthesis can be found in electronic supplementary material, file S6.

## 5.4. Immunofluorescence, TUNEL and EdU experiments

For immunofluorescence, larvae were relaxed, fixed and stored as for ISH, using PBS + 0.1% Tween-20 (PTw) instead of MFSW + 0.1% Tween-20 in the fixation buffers. Samples were rehydrated by decreasing concentrations of methanol in PTw (75%, 50%, 25%) and four 15-min washes in PTx (0.02% Triton X-100 in 1× PBS) at room temperature followed. Samples were then permeabilized with 0.3% Triton X-100 in 1× PBS for 20 min at room temperature and washed again three times with PTx prior to a blocking step of 3–5 h in 0.2 µm-filtered blocking solution (10% Bovine Serum Albumin -BSA-, 5% Normal Goat Serum -NGS-in 1X PBS). After blocking, samples were incubated overnight at 4°C in primary antibody anti-PH3 (anti-Histone H3 phospho-Ser10; Arigo Biolaboratories), anti-GH2A.X (Anti-phospho-Histone H2A.X (Ser139) Antibody, clone JBW301; EMD Millipore), or anti-Piwi1 [10] diluted 1 : 150, 1 : 200, or 1 : 100, respectively, in blocking solution. The following day, samples were washed four times for 10 min each in PTx + 5% BSA, followed by two long (1 h) washes in PTx + 5% BSA. Samples were then blocked again in fresh blocking solution for 1–3 h at room temperature, then incubated for 1 h at room temperature with secondary antibody Goat-anti-Rabbit 568 (Invitrogen) or Goat-anti-Mouse 488 (Invitrogen) at 1 : 500 dilution in blocking solution. Four washes of 30 min in PTx + 5% BSA followed, and samples were left washing in PTx + 5% BSA overnight at 4°C. The following day, samples were rinsed in PTx prior to nuclei staining.

For TUNEL assays, samples were relaxed as detailed above and fixed for 3 h at room temperature in TUNEL Fix (0.1 M Hepes, 0.05 M EGTA, 0.01 M $MgSO_4$, 0.02% Triton X-100 and 4% PFA in MFSW), followed by three 15-minute washes in PTw. Samples were dehydrated, stored, rehydrated, permeabilized, washed and blocked as for immunofluorescence, then rinsed in 1× PBS. For staining of apoptotic cells, we used the In Situ Cell Death Detection Kit Fluorescein (Millipore Sigma, 11684795910) following the manufacturer's recommendations. For positive controls, samples were incubated at 37°C for 20 min in two units of DNaseI diluted in 50 µl of 1× DNase buffer (from RNAqueous-Micro Total RNA Isolation Kit; Ambion), prior to TUNEL enzyme reaction.

To detect cells in S-phase of the cell cycle, EdU (Life Technologies C10340, Carlsbad, CA, USA) was added to solutions containing samples of interest, to a final concentration of 150 µM for different lengths of time, depending on sample type (5 min for 2 dpf and 3 dpf larvae; 10 min for primary polyps; 15 min for 8 dpf and 21 dpf larvae; 20 min for adult feeding and sexual polyps). Samples were then fixed, dehydrated, stored, rehydrated, permeabilized, washed and blocked as for immunofluorescence. The Click-iT EdU

detection reaction was carried out for 1 h at room temperature following the manufacturer's recommendations. When combined with immunofluorescence or fluorescent *in situ* hybridization, the Click-iT EdU detection reaction was performed at the end of the protocol, prior to nuclei staining.

In all cases, nuclei were stained using Hoechst 33342 and samples were mounted in Fluoromount (Sigma-Aldrich).

## 5.5. shRNA design, synthesis and electroporation

Design and synthesis of shRNAs targeting *GNL3* and a scrambled-*GNL3* control, as well as the electroporation procedure and survivorship assessment, were performed as previously described [40], with the exception that all electroporations were executed with a single shRNA at a concentration of 1500 ng $\mu l^{-1}$. Forward and reverse oligonucleotides of 66 bases in length that correspond to the DNA templates for shRNA *in vitro* transcription can be found in electronic supplementary material, file S7.

## 5.6. RT-qPCR and rRNA assessment

Larval RNA extraction, cDNA synthesis and qPCR analyses were performed as previously described [40]. Results were normalized to *Eef1alpha* housekeeping gene expression. Relative transcript expression levels of *GNL3* KDs were obtained using the delta-delta-ct method relative to scrambled shRNA controls. These relative expression levels are depicted as arbitrary units (arb. units) in figure 3. Three or more independent biological replicates were performed per experiment. Primer sequences are found in electronic supplementary material, file S7.

For rRNA assessment, larval RNA extraction was performed as previously described [40]. rRNA quality was checked using the Agilent 2100 Bioanalyzer. Results regarding rRNA levels and ratios are shown in electronic supplementary material, figure S8.

## 5.7. Generation of CRISPR/Cas9 mutant colonies

The three CRISPR sgRNAs targeting *GNL3* were designed using CRISPRscan, ordered from Synthego and resuspended in TE buffer (Synthego) at a concentration of 100–150 µM. sgRNAs were aliquoted and kept at −20°C until use. We avoided off-target matches by scanning the *Hydractinia* genome assembly at http://crispor.tefor.net. The sequences of the sgRNAs used in this study are found in electronic supplementary material, file S8. Cas9 protein (CP02; PNA BIO) was reconstituted in nuclease-free water to a concentration of 30 µM, aliquoted and kept at −80°C until use. Microinjection mixtures consisted of Cas9 protein at 6 µM, a combination of the three sgRNAs at approximately 5 µM concentration each, 100 mM KCl, and Dextran (Alexa Fluor 555; Invitrogen) at 1 mg $ml^{-1}$ concentration, all diluted in nuclease-free water. For Cas9-only controls, TE buffer (Synthego) was added instead of sgRNAs. Before microinjection, mixtures were incubated for 10 min at room temperature, then centrifuged at 14 000 r.p.m. for 10 min at room temperature. Within 80 min of spawning and following microinjection, eggs were fertilized and incubated at 28°C for 3 h to enhance Cas9 protein activity during early stages of development and then transferred to 18°C for the rest of the experiment. Injected embryos were cultured for 3 days in MFSW until larval metamorphosis was induced as previously described [40]. Only 4–5 metamorphosing larvae were added per slide, to allow colony growth assessment without a crowding effect and to avoid the fusion of neighbouring colonies. Slides with established primary polyps were transferred to aquariums to avoid algal growth and enhance stolonal expansion. Primary polyps were mouth-fed daily with smashed brine shrimp until colonies were large enough to be fed with whole nauplii. If two colonies of any experimental condition came into contact or fused, these were excluded from the analyses. Once colony growth data was collected (figure 4), a single colony on each slide was maintained as a founder for further experimentation.

## 5.8. Knockout genotyping

Following metamorphosis of individual larvae and colony growth analyses, 1–2 polyps per colony were taken for genomic DNA (gDNA) extraction. gDNA extraction buffer (0.01 M Tris pH8.0, 0.05 M KCl, 0.3% Tween-20, 0.3% NP40, 0.001 M EDTA, 0.5 mg $ml^{-1}$ Proteinase K [73]) was freshly prepared and placed on ice. Feeding polyps were dissected from the colony and placed inside the lid of a 0.5 ml PCR tube, where as much seawater as possible was removed before 20 µl of extraction buffer was pipetted on to the polyp. Tubes were centrifuged briefly before being placed at 55°C for 2–3 h, and vortexed every 30–60 min during incubation. Following incubation at 55°C, Proteinase K was inactivated by incubation at 98°C for 5 min. PCR was conducted using 5 µl or 10 µl of gDNA as input template with Takara ExTaq DNA polymerase (RR001A) and *GNL3*-specific primers that flanked the 3 predicted cut sites (electronic supplementary material, figure S9, S11 and file S8). Resulting fragments were analysed via agarose gel electrophoresis.

Three colonies (1.G2, 6.K2B and 6.F3L) were chosen for further analysis of CRISPR/Cas9-induced mutations. Following PCR and gel electrophoresis, bands of interest were excised and purified using the QIAquick Gel Extraction kit (Qiagen, Cat. #28704) and ligated into the pGEM-T Vector System (Promega, Cat. #A1360). Chemically competent DH5-alpha *E. coli* bacteria (ThermoFisher, EC0111) were transformed and plated on LB-agar plates containing ampicillin (100 µg $ml^{-1}$), IPTG (0.5 mM) and X-gal (80 µg $ml^{-1}$). Individual colonies were picked and verified to contain insert before being grown in overnight cultures of LB-broth containing ampicillin (100 µg $ml^{-1}$). Plasmid DNA was extracted using the Qiagen Miniprep Kit. Plasmid clones derived from individual bacterial colonies were Sanger-sequenced by Psomagen (https://psomagen.com/) using vector primers and analysed in Geneious to identify mutations.

## 5.9. Imaging, cell counting and stolonal area quantifications

Individual polyp and colony images were acquired with a digital camera (Zeiss Axiocam ERc 5 s) attached to a stereo microscope (Zeiss Stemi 508). Images of specimens from ISH experiments were taken with a digital camera (Zeiss Axiocam HRc) attached to a compound light microscope (Zeiss Imager.M2). Sperm motility videos were acquired with a Rolera EM-$C^2$ high-speed camera (QImaging) attached to a compound light microscope (Zeiss Imager.M2). Following

immunofluorescence, EdU labelling or fluorescent ISH, animals were imaged using a confocal microscope (Zeiss LSM 710). When comparisons between animals within an experiment were required, the same scanning parameters were used for all conditions of each independent experiment. All maximum intensity projections of z-stacks were generated using Fiji [74]. For quantification of cells that showed co-expression of *GNL3* with either *Piwi1*, *PCNA*, or those that had incorporated EdU, cells were manually counted in Fiji from confocal stacks after adjusting the images to enhance contrast, and processing images to reduce speckles. For $EdU^+$, $PH3^+$ and $Piwi1^+$ cell counting, larvae were compressed between the slide and cover slip to enable imaging of the full larval depth, and confocal z-stacks of approximately 10–15 µm were used. $EdU^+$ cells were highlighted using custom thresholding and counted using three-dimensional Object Counter in Fiji. $PH3^+$ and $Piwi1^+$ cells were manually counted in Fiji. For quantification of colony stolonal surface in *GNL3* KO experiments, light microscopy images were used. The animals' perimeters were outlined and areas were quantified using Fiji.

## 5.10. Graphs and statistics

Box plots in figure 3 and electronic supplementary material, figures S5 and S10 were generated using BoxPlotR [75]. The remaining graphs were designed in Excel and compiled using Adobe Illustrator.

For assessment of RT-qPCR statistical significance, we used the delta-Ct values, and performed Shapiro-Wilk tests to check for normality, followed by two-tailed Student's *t*-tests. For evaluation of 28 s/18 s rRNA ratio statistical significance, we first performed Shapiro–Wilk tests to check for normality, followed by two-tailed Student's *t*-tests. For statistics related to cell counting, normality was tested using Shapiro–Wilk tests, and Mann-Whitney *U* nonparametric tests were performed for two-way comparisons. Fisher's exact tests were chosen to analyse results of figure 4*b* based on 2 × 2 contingency tables. The statistical significance of stolonal area and polyp number comparisons between control and *GNL3* KO polyp colonies was determined by two-way ANOVA tests followed by *post hoc* Bonferroni corrections (electronic supplementary material, file S9). Statistical significance for all quantitative comparisons is indicated as *** where $p < 0.01$ and * where $p < 0.05$. Two-way comparison tests and Fisher's exact tests were conducted at http://www.socscistatistics.com, two-way ANOVA tests at http://www.statskingdom.com, and *post hoc* tests at http://www.graphpad.com.

Data accessibility. Accession numbers and source databases from the protein sequences used in figure 1*c* and electronic supplementary material, figure S2 are given in electronic supplementary material, table S1 [76].

Authors' contributions. G.Q.-A.: conceptualization, formal analysis, investigation, methodology, validation, visualization, writing—original draft, writing—review and editing; D.J.: formal analysis, investigation, methodology, validation, visualization, writing—review and editing; C.E.S.: conceptualization, funding acquisition, project administration, resources, supervision, validation, writing—review and editing.

All authors gave final approval for publication and agreed to be held accountable for the work performed therein.

Conflict of interest declaration. We declare we have no competing interests.

Funding. This work was funded by the NSF program 'Enabling Discovery through Genomics tools—EDGE' to C.E.S. (grant no. 1923259) and an NIH MIRA award to C.E.S. (grant no. R35GM138156).

Acknowledgements. We thank Dr Uri Frank for sending us an aliquot of the Piwi1 antibody, Dr Mark Martindale for sharing microinjection and microscopy equipment, Dr Leonardo Ibarra-Castro for helping to improve our *Hydractinia* and brine shrimp culture system, and Maddison Harman for the *Hydractinia* photo from figure 1.

# References

1. Martinez P *et al*. 2022 Articulating the 'stem cell niche' paradigm through the lens of non-model aquatic invertebrates. *BMC Biol.* **20**, 1–18. (doi:10.1186/s12915-022-01230-5)
2. Russell JJ *et al*. 2017 Non-model model organisms. *BMC Biol.* **15**, 55. (doi:10.1186/s12915-017-0391-5)
3. Goldstein B, King N. 2016 The future of cell biology: emerging model organisms. *Trends Cell Biol.* **26**, 818–824. (doi:10.1016/j.tcb.2016.08.005)
4. Technau U, Steele RE. 2012 Evolutionary crossroads in developmental biology: Cnidaria. *Development* **138**, 1447–1458. (10.1242/dev.048959)
5. Gold DA, Jacobs DK. 2013 Stem cell dynamics in Cnidaria: are there unifying principles? *Dev. Genes Evol.* **223**, 53–66. (doi:10.1007/s00427-012-0429-1)
6. Leclère L, Copley RR, Momose T, Houliston E. 2016 Hydrozoan insights in animal development and evolution. *Curr. Opin. Genet. Dev.* **39**, 157–167. (doi:10.1016/j.gde.2016.07.006)
7. Plickert G, Frank U, Müller WA. 2012 Hydractinia, a pioneering model for stem cell biology and reprogramming somatic cells to pluripotency. *Int. J. Dev. Biol.* **56**, 519–534. (doi:10.1387/ijdb.123502gp)
8. Gahan JM, Bradshaw B, Flici H, Frank U. 2016 The interstitial stem cells in *Hydractinia* and their role in regeneration. *Curr. Opin. Genet. Dev.* **40**, 65–73. (doi:10.1016/j.gde.2016.06.006)
9. Frank U, Nicotra ML, Schnitzler CE. 2020 The colonial cnidarian *Hydractinia*. *EvoDevo* **11**, 7–12. (doi:10.1186/s13227-020-00151-0)
10. DuBuc TQ *et al*. 2020 Transcription factor AP2 controls cnidarian germ cell induction. *Science* **367**, 757–762. (doi:10.1126/science.aay6782)
11. Bradshaw B, Thompson K, Frank U. 2015 Distinct mechanisms underlie oral vs aboral regeneration in the cnidarian *Hydractinia echinata*. *Elife* **2015**, e05506. (doi:10.7554/eLife.05506)
12. Millane RC, Kanska J, Duffy DJ, Seoighe C, Cunningham S, Plickert G, Frank U. 2011 Induced stem cell neoplasia in a cnidarian by ectopic expression of a POU domain transcription factor. **2439**, 2429–2439. (doi:10.1242/dev.064931)
13. Chrysostomou E *et al*. 2022 A cellular and molecular analysis of SoxB-driven neurogenesis in a cnidarian. *Elife* **11**, e78793. (doi:10.7554/elife.78793)
14. Tsai RY. 2011 New frontiers in nucleolar research: nucleostemin and related proteins. *Nucleolus* **15**, 301–320. (doi:10.1007/978-1-4614-0514-6_13)
15. Tsai RYL, Meng L. 2009 Nucleostemin: a latecomer with new tricks. *Int. J. Biochem. Cell Biol.* **41**, 2122–2124. (doi:10.1016/j.biocel.2009.05.020)
16. Tsai RYL, McKay RDG. 2002 A nucleolar mechanism controlling cell proliferation in stem cells and cancer cells. *Genes Dev.* **16**, 2991–3003. (doi:10.1101/gad.55671)
17. Tsai RYL. 2014 Turning a new page on nucleostemin and self-renewal. *J. Cell Sci.* **127**, 3885–3891. (doi:10.1242/jcs.154054)
18. Meng L, Zhu Q, Tsai RYL. 2007 Nucleolar trafficking of nucleostemin family proteins: common versus protein-specific mechanisms. *Mol. Cell. Biol.* **27**, 8670–8682. (doi:10.1128/mcb.00635-07)
19. Qu J, Bishop JM. 2012 Nucleostemin maintains self-renewal of embryonic stem cells and promotes reprogramming of somatic cells to pluripotency. *J. Cell Biol.* **197**, 731–745. (doi:10.1083/jcb.201103071)

20. Meng L, Lin T, Peng G, Hsu JK, Lee S, Lin SY, Tsai RYL. 2013 Nucleostemin deletion reveals an essential mechanism that maintains the genomic stability of stem and progenitor cells. *Proc. Natl Acad. Sci. USA* **110**, 11 415–11 420. (doi:10.1073/pnas.1301672110)
21. Hsu JK, Lin T, Tsai RYL. 2012 Nucleostemin prevents telomere damage by promoting PML-IV recruitment to SUMOylated TRF1. *J. Cell Biol.* **197**, 613–624. (doi:10.1083/jcb.201109038)
22. Romanova L, Grand A, Zhang L, Rayner S, Katoku-Kikyo N, Kellner S, Kikyo N. 2009 Critical role of nucleostemin in pre-rRNA processing. *J. Biol. Chem.* **284**, 4968–4977. (doi:10.1074/jbc.M804594200)
23. Essers PB, Pereboom TC, Goos YJ, Paridaen JT, MacInnes AW. 2014 A comparative study of nucleostemin family members in zebrafish reveals specific roles in ribosome biogenesis. *Dev. Biol.* **385**, 304–315. (doi:10.1016/j.ydbio.2013.10.029)
24. Lin T, Meng L, Lin TC, Wu LJ, Pederson T, Tsai RYL. 2014 Nucleostemin and GNL3L exercise distinct functions in genome protection and ribosome synthesis, respectively. *J. Cell Sci.* **127**, 2302–2312. (doi:10.1242/jcs.143842)
25. Meng L, Hsu JK, Tsai RYL. 2010 GNL3L depletion destabilizes MDM2 and induces p53-dependent G2/M arrest. *Oncogene* **30**, 1716–1726. (doi:10.1038/onc.2010.550)
26. Zhu Q, Meng L, Hsu JK, Lin T, Teishima J, Tsai RYL. 2009 GNL3L stabilizes the TRF1 complex and promotes mitotic transition. *J. Cell Biol.* **185**, 827–839. (doi:10.1083/jcb.200812121)
27. Fu D, Collins K. 2007 Purification of human telomerase complexes identifies factors involved in telomerase biogenesis and telomere length regulation. *Mol. Cell* **28**, 773–785. (doi:10.1016/j.molcel.2007.09.023)
28. Yasumoto H, Meng L, Lin T, Zhu Q, Tsai RYL. 2007 GNL3L inhibits activity of estrogen-related receptor $\gamma$ by competing for coactivator binding. *J. Cell Sci.* **120**, 2532–2543. (doi:10.1242/jcs.009878)
29. Tarashansky AJ, Musser JM, Khariton M, Li P, Arendt D, Quake SR, Wang B. 2021 Mapping single-cell atlases throughout metazoa unravels cell type evolution. *Elife* **10**, e66747. (doi:10.7554/eLife.66747)
30. Bassler J, Grandi P, Gadal O, Lessmann T, Petfalski E, Tollervey D, Lechner J, Hurt E. 2001 Identification of a 60S preribosomal particle that is closely linked to nuclear export. *Mol. Cell* **8**, 517–529. (doi:10.1016/S1097-2765(01)00342-2)
31. Du X, Subba Rao MRK, Chen XQ, Wu W, Mahalingam S, Balasundaram D. 2006 The homologous putative GTPases Grn1p from fission yeast and the human GNL3L are required for growth and play a role in processing of nucleolar pre-rRNA. *Mol. Biol. Cell* **17**, 460–474. (doi:10.1091/mbc.E05-09-0848)
32. Rosby R, Cui Z, Rogers E, Delivron MA, Robinson VL, Dimario PJ. 2009 Knockdown of the *Drosophila* GTPase, nucleostemin 1, impairs large ribosomal subunit biogenesis, cell growth, and midgut precursor cell maintenance. *Mol Biol Cell* **20**, 4424–4434 (doi:10.1091/mbc.e08-06-0592)
33. Kudron MM, Reinke V. 2008 C. elegans nucleostemin is required for larval growth and germline stem cell division. *PLoS Genet.* **4**, e1000181. (doi:10.1371/journal.pgen.1000181)
34. Reddien PW, Bermange AL, Murfitt KJ, Jennings JR, Sánchez Alvarado A. 2005 Identification of genes needed for regeneration, stem cell function, and tissue homeostasis by systematic gene perturbation in planaria. *Dev. Cell* **8**, 635–649. (doi:10.1016/j.devcel.2005.02.014)
35. Wang X, Gingrich DK, Deng Y, Hong Z. 2012 A nucleostemin-like GTPase required for normal apical and floral meristem development in *Arabidopsis*. *Mol. Biol. Cell* **23**, 1446–1456. (doi:10.1091/mbc.E11-09-0797)
36. Wang X, Xie B, Zhu M, Zhang Z, Hong Z. 2012 Nucleostemin-like 1 is required for embryogenesis and leaf development in *Arabidopsis*. *Plant Mol. Biol.* **78**, 31–44. (doi:10.1007/s11103-011-9840-7)
37. Wang Z, Wang X, Xie B, Hong Z, Yang Q. 2018 *Arabidopsis* NUCLEOSTEMIN-LIKE 1 (NSN1) regulates cell cycling potentially by cooperating with nucleosome assembly protein AtNAP1;1. *BMC Plant Biol.* **18**, 1–12. (doi:10.1186/s12870-018-1289-2)
38. Jeon Y, Park YJ, Cho HK, Jung HJ, Ahn TK, Kang H, Pai HS. 2015 The nucleolar GTPase nucleostemin-like 1 plays a role in plant growth and senescence by modulating ribosome biogenesis. *J. Exp. Bot.* **66**, 6297–6310. (doi:10.1093/jxb/erv337)
39. Müller WA, Teo R, Frank U. 2004 Totipotent migratory stem cells in a hydroid. *Dev. Biol.* **275**, 215–224. (doi:10.1016/j.ydbio.2004.08.006)
40. Quiroga-Artigas G, Duscher A, Lundquist K, Waletich J, Schnitzler CE. 2020 Gene knockdown via electroporation of short hairpin RNAs in embryos of the marine hydroid Hydractinia symbiolongicarpus. *Sci. Rep.* **10**, 1–15. (doi:10.1038/s41598-020-69489-8)
41. Scully R, Xie A. 2013 Double strand break repair functions of histone H2AX. *Mutat. Res. Fundam. Mol. Mech. Mutagen.* **750**, 5–14. (doi:10.1016/j.mrfmmm.2013.07.007)
42. Reddy PC, Ubhe S, Sirwani N, Lohokare R, Galande S. 2017 Rapid divergence of histones in Hydrozoa (Cnidaria) and evolution of a novel histone involved in DNA damage response in hydra. *Zoology* **123**, 53–63. (doi:10.1016/j.zool.2017.06.005)
43. Singh A, Xu YJ. 2016 The cell killing mechanisms of hydroxyurea. *Genes (Basel).* **7**, 99. (doi:10.3390/genes7110099)
44. Gahan JM *et al*. 2017 Functional studies on the role of Notch signaling in *Hydractinia* development. *Dev. Biol.* **428**, 224–231. (doi:10.1016/j.ydbio.2017.06.006)
45. Beekman C, Nichane M, De Clercq S, Maetens M, Floss T, Wurst W, Bellefroid E, Marine J-C. 2006 Evolutionarily conserved role of nucleostemin: controlling proliferation of stem/progenitor cells during early vertebrate development. *Mol. Cell. Biol.* **26**, 9291–9301. (doi:10.1128/mcb.01183-06)
46. Wang J, Wang L, Ji Q, Zhu H, Han S. 2017 Knockdown of Nucleostemin in an ovarian cancer SKOV-3 cell line and its effects on cell malignancy. *Biochem. Biophys. Res. Commun.* **487**, 262–267. (doi:10.1016/j.bbrc.2017.04.046)
47. Zhang Y, Wang Y, Meng L, Huang Q, Zhu Y, Cui W, Cheng Y, Liu R. 2021 Targeted micelles with chemotherapeutics and gene drugs to inhibit the G1/S and G2/M mitotic cycle of prostate cancer. *J. Nanobiotechnol.* **19**, 1–15. (doi:10.1186/s12951-020-00756-6)
48. Birnbaum KD, Alvarado AS. 2008 Slicing across kingdoms: regeneration in plants and animals. *Cell* **132**, 697–710. (doi:10.1016/j.cell.2008.01.040)
49. Alvarado AS, Tsonis PA. 2006 Bridging the regeneration gap: genetic insights from diverse animal models. *Nat. Rev. Genet.* **7**, 873–884. (doi:10.1038/nrg1923)
50. Wenemoser D, Reddien PW. 2010 Planarian regeneration involves distinct stem cell responses to wounds and tissue absence. *Dev. Biol.* **344**, 979–991. (doi:10.1016/j.ydbio.2010.06.017)
51. Wagner DE, Wang IE, Reddien PW. 2011 Clonogenic neoblasts are pluripotent adult stem cells that underlie planarian regeneration. *Science* **332**, 811–816. (doi:10.1126/science.1203983)
52. Reber-Müller S, Streitwolf-Engel R, Yanze N, Schmid V, Stierwald M, Erb M, Seipel K. 2006 BMP2/4 and BMP5-8 in jellyfish development and transdifferentiation. *Int. J. Dev. Biol.* **50**, 377–384. (doi:10.1387/ijdb.052085sr)
53. Maki N, Takechi K, Sano S, Tarui H, Sasai Y, Agata K. 2007 Rapid accumulation of nucleostemin in nucleolus during newt regeneration. *Dev. Dyn.* **236**, 941–950. (doi:10.1002/dvdy.21027)
54. Tanaka EM, Reddien PW. 2011 The cellular basis for animal regeneration. *Dev. Cell* **21**, 172–185. (doi:10.1016/j.devcel.2011.06.016)
55. Li T, Li L, Wu X, Tian K, Wang Y. 2019 The oncogenic role of GNL3 in the progression and metastasis of osteosarcoma. *Cancer Manag. Res.* **11**, 2179–2188. (doi:10.2147/CMAR.S195360)
56. Ohmura M *et al.* 2008 Identification of stem cells during prepubertal spermatogenesis via monitoring of nucleostemin promoter activity. *Stem Cells* **26**, 3237–3246. (doi:10.1634/stemcells.2008-0506)
57. Malone JH, Chrzanowski TH, Michalak P. 2007 Sterility and gene expression in hybrid males of *Xenopus laevis* and *X. muelleri*. *PLoS ONE* **2**, e0000781. (doi:10.1371/journal.pone.0000781)
58. Nikpour P, Mowla SJ, Jafarnejad SM, Fischer U, Schulz WA. 2009 Differential effects of Nucleostemin suppression on cell cycle arrest and apoptosis in the bladder cancer cell lines 5637 and SW1710. *Cell Prolif.* **42**, 762–769. (doi:10.1111/j.1365-2184.2009.00635.x)
59. Liu R, Zhang Z, Xu Y. 2010 Downregulation of nucleostemin causes G1 cell cycle arrest via a p53-independent pathway in prostate cancer PC-3 cells. *Urol. Int.* **85**, 221–227. (doi:10.1159/000315968)
60. Jafarnejad SM, Mowla SJ, Matin MM. 2008 Knocking-down the expression of nucleostemin significantly decreases rate of proliferation of rat

bone marrow stromal stem cells in an apparently p53-independent manner. *Cell Prolif.* **41**, 28–35. (doi:10.1111/j.1365-2184.2007.00505.x)

61. Huang G, Meng L, Tsai R. 2015 p53 Configures the G2/M arrest response of nucleostemin-deficient cells. *Cell Death Discov.* **1**, 1–8. (doi:10.1038/cddiscovery.2015.60)
62. Yamashita M, Nitta E, Nagamatsu G, Ikushima YM, Hosokawa K, Arai F, Suda T. 2013 Nucleostemin is indispensable for the maintenance and genetic stability of hematopoietic stem cells. *Biochem. Biophys. Res. Commun.* **441**, 196–201. (doi:10.1016/j.bbrc.2013.10.032)
63. Rahmati M, Moosavi MA, Zarghami N. 2014 Nucleostemin knocking-down causes cell cycle arrest and apoptosis in human T-cell acute lymphoblastic leukemia MOLT-4 cells via p53 and p21Waf1/Cip1 up-regulation. *Hematology* **19**, 455–462. (doi:10.1179/1607845414Y.0000000153)
64. Nomura J *et al.* 2009 Differential requirement for nucleostemin in embryonic stem cell and neural stem cell viability. *Stem Cells* **27**, 1066–1076. (doi:10.1002/stem.44)
65. Paridaen JTML, Janson E, Utami KH, Pereboom TC, Essers PB, van Rooijen C, Zivkovic D, MacInnes AW. 2011 The nucleolar GTP-binding proteins Gnl2 and nucleostemin are required for retinal neurogenesis in developing zebrafish. *Dev. Biol.* **355**, 286–301. (doi:10.1016/j.ydbio.2011.04.028)
66. Seipp S, Schmich J, Leitz T. 2001 Apoptosis: a death-inducing mechanism tightly linked with morphogenesis in *Hydractina echinata* (Cnidaria, Hydrozoa). *Development* **128**, 4891–4898. (doi:10.1242/dev.128.23.4891)
67. Frickey T, Lupas A. 2004 CLANS: a Java application for visualizing protein families based on pairwise similarity. *Bioinformatics* **20**, 3702–3704. (doi:10.1093/bioinformatics/bth444)
68. Fu L, Niu B, Zhu Z, Wu S, Li W. 2012 CD-HIT: accelerated for clustering the next-generation sequencing data. *Bioinformatics* **28**, 3150–3152. (doi:10.1093/bioinformatics/bts565)
69. Katoh K, Standley DM. 2013 MAFFT multiple sequence alignment software version 7: improvements in performance and usability. *Mol. Biol. Evol.* **30**, 772–780. (doi:10.1093/molbev/mst010)
70. Darriba D, Taboada GL, Doallo R, Posada D. 2011 ProtTest 3: fast selection of best-fit models of protein evolution. *Bioinformatics* **27**, 1164–1165. (doi:10.1093/bioinformatics/btr088)
71. Guindon S, Gascuel O. 2003 A simple, fast, and accurate algorithm to estimate large phylogenies by maximum likelihood. *Syst. Biol.* **52**, 696–704. (doi:10.1080/10635150390235520)
72. Stamatakis A. 2014 RAxML version 8: a tool for phylogenetic analysis and post-analysis of large phylogenies. *Bioinformatics* **30**, 1312–1313. (doi:10.1093/bioinformatics/btu033)
73. Ikmi A, McKinney SA, Delventhal KM, Gibson MC. 2014 TALEN and CRISPR/Cas9-mediated genome editing in the early-branching metazoan *Nematostella vectensis*. *Nat. Commun.* **5**, 1–8. (doi:10.1038/ncomms6486)
74. Schneider CA, Rasband WS, Eliceiri KW. 2012 NIH Image to ImageJ: 25 years of image analysis. *Nat. Methods* **9**, 671–675. (doi:10.1038/nmeth.2089)
75. Spitzer M, Wildenhain J, Rappsilber J, Tyers M. 2014 BoxPlotR: a web tool for generation of box plots. *Nat. Methods* **11**, 121–122. (doi:10.1038/nmeth.2811)
76. Quiroga-Artigas G, de Jong D, Schnitzler CE. 2022 *GNL3* is an evolutionarily conserved stem cell gene influencing cell proliferation, animal growth and regeneration in the hydrozoan *Hydractinia*. Figshare. (doi:10.6084/m9.figshare.c.6167574)